INSTITUTE FOR FUSION STUDIES

DOE/ET-53088-436 IFSR #436

$m = 1$ Kink Mode for Layer Widths Comparable to the Ion Larmor Radius

H.L. BERK, S.M. MAHAJAN, and Y.Z. ZHANG
Institute for Fusion Studies
The University of Texas at Austin
Austin, Texas 78712

August 1990

THE UNIVERSITY OF TEXAS

AUSTIN

$m = 1$ Kink Mode for Layer Widths Comparable to the Ion Larmor Radius

H.L. Berk, S.M. Mahajan, and Y.Z. Zhang
Institute for Fusion Studies
The University of Texas at Austin
Austin, Texas 78712

Abstract

A kink-tearing eigenmode equation is derived for a slab layer geometry in the limit $m_e/m_i \ll \beta_i \ll L_n^2/L_s^2$ ($m_e/m_i \equiv$ mass ratio, $\beta_i \equiv$ ion beta value, $L_n \equiv$ gradient scale length, $L_s \equiv$ shear length) and when the electron collision frequency is comparable to the eigenfrequency. It is essential for consistency to retain arbitrary ion Larmor radius effects, which are described with the use of the Padé approximation. The asymptotic solution of the inhomogeneous eigenvalue problem is obtained using simple approximations to the eigenfunction. A dispersion relation duplicates previously derived results when a Lorentzian conductivity model is used for electrons, while a new dispersion relation is obtained if electrons are described by kinetic dynamics. The dispersion relation is analytically and numerically investigated. The numerical results are compared to a more complicated and presumably more "rigorous" asymptotic expression. It is shown that this asymptotic expression requires quite small value for $(m_e/m_i)\beta_i$ for accuracy. A fitting formula is found that is more accurate than the asymptotic formula for moderate values of $(m_e/m_i)\beta_i$. The dissipationless dispersion relation is discussed and it is shown that local shear at the $q = 1$ surface can have a stronger effect than the value of $\delta\widehat{W}_c$ (the MHD energy) on the system's stability properties.

When stability is predicted, electron dissipation due to collisions or electron Landau damping destabilizes a low frequency negative energy mode that is present. Electron temperature gradients are shown to reduce Landau damping and thus decreases the destabilizing drive on the negative energy mode.

I. Introduction

There have been many studies of the $m = 1$ internal kink mode and its relation with sawtooth activity observed in tokamaks.[1–4] This mode is also believed to play an important role in experiments with auxiliary heating in tokamaks, e.g., the fishbone instabilities[5,6] and the suppression of sawteeth.[7–11]

Theories, including hot particles created by auxiliary heating, have been formed to explain both the stabilizing aspect (sawtooth suppression) and the destabilizing aspect (fishbone).[12–18] In these theories the main emphasis is placed on the consideration of the dynamics of hot particles, while for the layer dynamics simplified theories are used that are based on ideal or resistive MHD (magnetohydrodynamics) theory. It has been found in these theoretical investigations that there is a broad parameter region where the $m = 1$ mode with hot particles oscillates near the ion diamagnetic drift frequency ω_i^*. In fact, it has been pointed out[19] that in the high temperature regime the ion Larmor radius, ρ_i, can be greater than the Alfvén layer width $x_A r_s$, where x_A^2 is defined as $x_A^2 \equiv \omega(\omega - \omega_i^*)/\omega_A^2$ with $\omega_A = (v_A/Rq)(r_s/q)(dq/dr)$, in which v_A is the Alfvén speed, R is the major radius, r_s is the radius of the rational surface, and q is the safety factor ($q = 1$ for the $m = 1$ mode). Thus, if the mode frequency, ω, approaches to ω_i^*, the ion Larmor radius can be greater than the Alfvén layer width. As a result, the mode tends to localize over distance ρ_i rather than $x_A r_s$. The response of the system can then be significantly altered, and in particular, the dissipation due to the Alfvén resonance is greatly reduced. This situation forces a different approach to describing the layer dynamics in order to take into account the important finite Larmor radius effects and the electron dynamics in the kink layer of the mode. It is this aspect of the theory which will be emphasized in this paper. In a later work we will apply the layer equations developed here to describe the effect of hot particles on the kink mode.

The $m = 1$ kink-tearing mode with FLR effects in absence of the hot particles has been

studied by several authors.[20–28] Generally, the problem of including both ion and electron kinetic effects is difficult to treat. However, if electron Landau damping is approximated by a Lorentzian conductivity model [cf. Eqs. (A1)–(A2)], and the Bessel functions in ion FLR effects is mathematically modeled by the Padé approximation [cf. Eq. (11)], a homogeneous second order differential equation can be derived in the Fourier transformed space (k).The MHD driving term does not appear in the equation and enters as a boundary condition in the small k region.[20–25] The dispersion relation following this approach has been obtained by Chen and Hahm,[20,21] and Pegoraro, Porcelli and Schep.[22–24] Recently, Pegoraro *et al.* extend this approach to include the finite ion temperature gradient.[25] On the other hand, the kink-tearing problem with both ion and electron kinetic effects can also be solved in other approximation.[5] Coppi *et al.*,[26,27] and Cowley *et al.*[28] solved the coupled integral equations by using the constant-Ψ approximation, which however is not plausible for the $m = 1$ mode. Zhang, Berk, and Mahajan derived variational forms for the coupled integral equation, which was solved in the large conductivity limit.[19] Since the validity of solution by variational approach is crucially dependent on the choice of trial function, it is important to choose the correct trial function which can alter considerably in different parameter regimes.

In this paper we consider in detail the parameter regime $m_e/m_i \ll \beta_i \ll L_n^2/L_s^2$, where L_n and L_s are the density and magnetic shear scale lengths on the resonant surface. In this regime simple eigenfunctions are justified and electron dynamics that are described by kinetic theory effects of the layer can be treated. Ion FLR effects are also described using the Padé approximation, which has been shown to be a good one in Ref. 25 as long as ion temperature gradient can be ignored. Use of the Padé approximation enables us to derive an inhomogeneous eigenmode equation, which is formally similar to that given by Mahajan *et al.* in the small Larmor radius limit.[29] This derivation is shown in Sec. II and in Appendix A. When a Lorentzian model is used for the electron conductivity, the dispersion relation is found to be identical to that obtained earlier by other authors.[24,25] This derivation is shown

in Sec. III.

The dispersion relation without hot particles is analyzed and numerically solved in Sec. IV. When $T_e/T_i \ll 1$ there are four distinct modes; one mode is in the electron direction, while the other three modes are in the ion direction. This is in contrast with the small Larmor radius theory, where there exist only two distinct modes in the ion direction.[13] One of the three modes in the ion direction is a drift type mode with $\omega \sim \omega_i^*$. The mode in the electron direction is also a drift type with $\omega \sim \omega_e^*$ (ω_e^* is the electron diamagnetic frequency). Both the drift modes are stable modes, and may be related to those discussed by Coppi *et al.*,[26,27] and Cowley *et al.*[28] The other two modes (in the ion direction) appear to be a pair of conjugate modes, which connect to the MHD branch. For finite T_e/T_i the mode structure is more complex. Marginal stability diagrams are determined. Marginal modes where $0 < \omega/\omega_e^* < 1$ are found with the instability region corresponding to the positive (i.e. the supposedly stable) MHD energy. Electron collisions appear to eliminate any completely stable region.

The numerical results show that kinetic electron dynamics yield quantitative rather than a qualitative differences from the results obtained from a Lorentzian conductivity model for electrons. An electron temperature gradient is found to weaken the destabilization mechanism of the negative energy waves. We will not discuss the effects of hot particles on the FLR kink mode in this paper; discussion of these results will appear in a later work.

II. Derivation of the Inhomogeneous Eigenmode Equation in Padé Approximation

The basic equations describing the layer dynamics of the FLR kink-tearing eigenmode in a slab model are obtained from the vorticity equation and Ohm's law,[26,28] and are given by

$$x_A^2 \frac{d}{dx} \int dx' \, \tilde{G}(x-x') \frac{d}{dx'} \xi(x') = x \frac{d^2\psi}{dx^2} = \frac{d}{dx}\left(x \frac{d\psi}{dx} - \psi \right) , \qquad (1)$$

$$\frac{d^2\psi}{dx^2} = \frac{\sigma(x)}{x^2}\, E(x)\ , \tag{2}$$

where integrals throughout this section vary from $-\infty$ to ∞, the parallel electric field is $E(x) = \psi(x) - x\xi(x)$,

$$\tilde{G}(x - x') \equiv \int \frac{dk}{2\pi}\, e^{ik(x-x')} \tilde{G}_k \tag{3}$$

with

$$\tilde{G}_k \equiv \frac{1}{b_k}\,[1 - \Gamma_0(b_k)] + \frac{\omega_{iT}^*}{\omega - \omega_{in}^*}\,[\Gamma_1(b_k) - \Gamma_0(b_k)]\ , \tag{4}$$

$b_k \equiv \frac{1}{2}\,\widehat{\rho}_i^{\,2}\,k^2$, $\Gamma_n(b) = e^{-b} I_n(b)$, I_n is the nth order of modified Bessel function, ω_{in}^* and ω_{iT}^* is the ion diamagnetic frequency due to density and temperature gradient respectively, $\widehat{\rho}_i \equiv \rho_i / r_s$ with r_s the radial position of the $q = 1$ rational surface and $\rho_i \equiv \omega_i c v_i / eB$ is the ion Larmor radius (we define the thermal ion velocity v_i by $\sqrt{2T_i/m_i}$ throughout this paper). Further, for a collisionless kinetic electron model we have

$$\sigma(x) \equiv -\sigma_0\, \Pi(x) \tag{5}$$

in which

$$\sigma_0 \equiv \left(\frac{r_s}{\rho_s}\right)^2 \frac{\omega(\omega - \omega_{en}^*)}{\omega_A^2}\ ,$$

and

$$\Pi(x) = \equiv [1 + \zeta_e Z(\zeta_e)] - \frac{\omega_{eT}^*}{\omega - \omega_{en}^*}\,\zeta_e \left[\zeta_e + \zeta_e^2\, Z(\zeta_e) - \frac{1}{2}\, Z(\zeta_e)\right] \tag{6}$$

with ω_{en}^* and ω_{eT}^* the electron diamagnetic frequency due to density and temperature gradient respectively, Z is the plasma dispersion function, $\zeta_e \equiv x_e/|x|$, $x_e \equiv \omega/k_\parallel' v_e$, $k_\parallel' \equiv 1/L_s$, $x = (r - r_s)/r_s$, L_s is the shear length, v_e the electron thermal velocity $\left(v_e = \sqrt{2T_e/m_e}\right)$, and $\rho_s^2 \equiv T_e\, m_i c^2 / e^2 B^2$ and ω_A is the Alfvén frequency ($\omega_A \equiv k_\parallel' v_A$, with the Alfvén speed defined by $v_A^2 \equiv B^2/4\pi\, m_i n$).

In the slab model the boundary condition at large x for the kink mode is obtained using the assumption that the parallel electric field E vanishes outside the $q = 1$ layer region,[4] which gives for large $|x|$

$$\xi(x) \to \xi(-\infty)\left[\theta(-x) - \frac{1}{\Delta' x}\right] , \tag{7}$$

$$\psi(x) \to x\xi(-\infty)\left[\theta(-x) - \frac{1}{\Delta' x}\right] , \tag{8}$$

where $\theta(x)$ is the Heaviside step function and Δ' is given by the standard definition of the kink-tearing problem. For the $m = 1$ mode[4] $\Delta' = \pi/\delta\widehat{W}$, where $\delta\widehat{W}$ is the normalized bulk plasma perturbed energy found from an energy principle. For example, in absence of hot particles, using the Bussac formula,[1] it is found in the large aspect ratio limit

$$\delta\widehat{W} = \delta\widehat{W}_c = 3(1 - q(0))\left(\frac{13}{144} - \tilde{\beta}_p^2\right)\left(\frac{r_s}{R}\right)^2 , \tag{9}$$

where $q(0)$ is the safety factor of tokamak at $r = 0$, R the major radius of the tokamak,

$$\tilde{\beta}_p = \left(\frac{8\pi}{B_p^2}\right)\int_0^{r_s/a} dy\, y\left(\frac{dP}{dy}\right) , \tag{10}$$

where a is the minor radius of the tokamak plasma, B the poloidal field at $q = 1$ surface, P is the isotropic plasma pressure. $\delta\widehat{W}$ can also be modified due to the presence of hot particles in the plasma, so that $\delta\widehat{W} = \delta\widehat{W}_c + \delta\widehat{W}_k$. The expression for $\delta\widehat{W}_k$ (the kinetic contribution to the perturbed energy) has been calculated in several works.[12,16,18,30]

Now we introduce the Padé approximation for the description of arbitrary ion Larmor radius effect. A simple form can be obtained when $\omega_{iT}^* = 0$, wherein $\tilde{G}_k = [1 - \Gamma_0(b_k)]/b_k$ in Eq. (4) is replaced by

$$\tilde{G}_k = \frac{1}{1 + b_k} , \tag{11}$$

which is an interpolation form that matches the large and small b_k limit. Making use of Eq. (11), we obtain the explicit expression for $\tilde{G}(x - x')$ in the Padé approximation

$$\tilde{G}(x - x') = \frac{1}{\sqrt{2}\,\widehat{\rho}_i}\exp\left(-\frac{\sqrt{2}}{\widehat{\rho}_i}|x - x'|\right) , \tag{12}$$

which satisfies the equation

$$\frac{\widehat{\rho}_i^2}{2}\frac{d^2}{dx^2}\tilde{G}(x-x') - \tilde{G}(x-x') = -\delta(x-x') \; . \tag{13}$$

We note that the first integral of Eq. (1), with the boundary condition Eqs. (6) and (7), yields the expression

$$x_A^2 \int dx' \, \tilde{G}(x-x')\chi(x') = x^2 \frac{d}{dx}\left(\frac{E}{x}\right) + x^2\chi(x) + \frac{1}{\Delta'}\int dx \, \chi(x) \tag{14}$$

with $\chi(x) \equiv d\xi/dx$. In Eq. (14) the constant of integration was found by noting that from Eq. (7) we must have $\dfrac{d\xi(\infty)}{dx} \to \xi(-\infty)/\Delta' x^2$ for large $|x|$. This limit is recovered in Eq. (14) if we note that for large $|x|$ the left-hand side and the first term on the right-hand side is $\mathcal{O}(1/x^2)$ for large x, while the last two terms on the right-hand side of Eq. (14) are constant that reproduce the relation for $d\xi/dx$ at large $|x|$.

Now applying the operator $(\widehat{\rho}_i^2/2)(d^2/dx^2)$ on Eq. (14), and using Eq. (13), we obtain

$$\frac{\widehat{\rho}_i^2}{2}\frac{d^2}{dx^2}x^2\chi(x) + (x_A^2 - x^2)\chi(x) - \frac{1}{\Delta'}\int dx \, \chi(x) - x^2\frac{d}{dx}\left(\frac{E}{x}\right)$$
$$+ \frac{\widehat{\rho}_i^2}{2}\frac{d^2}{dx^2}x^2\frac{d}{dx}\left(\frac{E}{x}\right) = 0 \; . \tag{15}$$

Substituting Eq. (2), written in the form

$$\frac{d^2E}{dx^2} - \frac{\sigma(x)}{x^2}E(x) = -\frac{1}{x}\frac{d}{dx}x^2\chi(x) \; , \tag{16}$$

we obtain

$$\chi(x) = \frac{1}{x^2 - x_A^2}\left(-\frac{1}{\Delta'}\int dx \, \chi(x)\right) - \frac{x^2}{x^2 - x_A^2}\frac{d}{dx}\left(\frac{E}{x}\right)$$
$$+ \frac{1}{x^2 - x_A^2}\cdot\frac{\widehat{\rho}_i^2}{2}\frac{d}{dx}\frac{\sigma(x)}{x}E(x) \; . \tag{17}$$

Integrating over x then yields

$$\frac{1}{\Delta'}\int dx \, \chi(x) = \frac{1}{\Delta' + \dfrac{i\pi}{x_A}}\int dx \, \frac{E(x)}{(x^2 - x_A^2)^2}\left[\widehat{\rho}_i^2\sigma(x) - 2x_A^2\right] \; . \tag{18}$$

Equation (18) is then substituted into Eq. (17) to obtain $\chi(x)$ in terms of $E(x)$. If this expression is substituted into Eq. (16) we obtain, after defining

$$\Psi(x) \equiv \left[1 - \frac{\widehat{\rho}_i^2 \sigma(x)}{2x_A^2}\right] E(x) \ , \tag{19}$$

an eigenmode equation for $\Psi(x)$

$$\frac{d}{dx}\frac{1}{x^2 - x_A^2}\frac{d}{dx}\Psi(x) + \frac{2}{(x^2 - x_A^2)^2}\Psi(x) + \frac{\sigma(x)}{x^2 x_A^2\left[1 - \frac{\widehat{\rho}_i^2\sigma(x)}{2x_A^2}\right]}\Psi(x)$$

$$+ \frac{1}{\Delta' + \frac{i\pi}{x_A}}\frac{4x_A^2}{(x^2 - x_A^2)^2}\int dx \frac{\Psi(x)}{(x^2 - x_A^2)^2} = 0 \ . \tag{20}$$

Defining $Q(x) \equiv \Psi(x)/x$, we find that Eq. (20) is almost the same form of the equation derived by Mahajan *et al.*,[29] except an extra factor $\widehat{\rho}_i^2\sigma(x)/2x_A^2$ in the third term on the left-hand side of Eq. (20), which formally arises from the inclusion of the arbitrary ion Larmor radius terms. It is interesting that the structural form of Eq. (20) does not change with ion FLR effects included even when the mode width is comparable to an ion Larmor radius. The kink-tearing eigenmode equation remains second order, and formally only the effective electron conductivity is modified. Explicitly, we express for $\omega_{eT}^* = 0$

$$\frac{\widehat{\rho}_i^2\sigma(x)}{2x_A^2} = -\frac{T_i}{T_e}\frac{\omega - \omega_e^*}{\omega - \omega_i^*}\left[1 + \zeta_e Z(\zeta_e)\right] \ . \tag{21}$$

Since $1 + \zeta_e Z(\zeta_e)$ is order unity except in the innermost region ($x \ll x_e$), we conclude that for the mode $\omega \sim \omega_e^*$ with $|\omega/\omega_e^* - 1| \ll 1$, the FLR effects can be important only due to finite η_e, the ratio of electron temperature to density gradient. However, for the mode $\omega \sim \omega_i^*$ the FLR is important, in particular, for $|1 - \omega/\omega_i^*| \ll 1$ the conductivity term is greatly modified by the FLR except in a very small region $x \sim 0$.

A variational form for the trial function $\Psi(x)$ can be easily constructed from Eq. (20) by multiplying by Ψ and integrating over all space, to obtain

$$S[\Psi] = -\int dx \frac{1}{x^2 - x_A^2}\left(\frac{d\Psi}{dx}\right)^2 + 2\int dx \frac{\Psi^2(x)}{(x^2 - x_A^2)^2}$$

$$+\frac{1}{x_A^2}\int dx\,\frac{\sigma(x)\Psi^2(x)}{x^2\left[1-\dfrac{\widehat{\rho}_i^2\sigma(x)}{2x_A^2}\right]}+\frac{4x_A^2}{\Delta'+\dfrac{i\pi}{x_A}}\left[\int dx\,\frac{\Psi(x)}{(x^2-x_A^2)^2}\right]^2=0\ . \qquad (22)$$

Note that Eq. (20) is the Euler equation of Eq. (22).

III. Dispersion Relation

A dispersion relation can be obtained from the quadratic form with a good approximate test function. To understand the mathematical structure of the inhomogeneous eigenvalue problem we prefer to transform Eq. (20) into a formally real form by defining the following variables: $y \equiv ix/x_A$, $y_e \equiv x_e/x_A$, $\widetilde{\rho}^2 \equiv \sigma_0\widehat{\rho}_i^2/2x_A^2$, and $\Delta = i\Delta' x_A$. Equation (20) is then rewritten as

$$\frac{d}{dy}\frac{1}{y^2+1}\frac{d}{dy}\Psi+\frac{2}{(y^2+1)^2}\Psi+\frac{\sigma_0 g(y/y_e)}{y^2[1+\widetilde{\rho}^2 g(y/y_e)]}\Psi$$
$$+\frac{1}{\Delta-\pi}\cdot\frac{8}{(y^2+1)^2}\int_0^\infty dy\,\frac{\Psi(y)}{(y^2+1)^2}=0\ , \qquad (23)$$

where $g(y/y_e) \equiv \Pi(-iy/y_e)$ ($\Pi(x)$ is defined by Eq. (6).) Since in general $i(y_e/y)Z(iy_e/y)$ is a real function for real y/y_e, $g(y/y_e)$ is also real for real y/y_e. The quadratic form Eq. (22) is rewritten as

$$\sigma_0=\frac{\displaystyle\int_0^\infty dy\left[\frac{(d\Psi/dy)^2}{y^2+1}-\frac{2\Psi^2}{(y^2+1)^2}\right]+\frac{8}{\pi-\Delta}\left[\int_0^\infty dy\,\frac{\Psi(y)}{(y^2+1)^2}\right]^2}{\displaystyle\int_0^\infty dy\,\frac{g(y/y_e)\Psi^2(y)}{y^2[1+\widetilde{\rho}^2 g(y/y_e)]}}\ , \qquad (24)$$

where σ_0 can be viewed as the "eigenvalue" of Eq. (24) for given Δ, $\widetilde{\rho}$, and y_e.

For a Lorentzian conductivity model, in which $g(y/y_e) = (y/y_e)^2/[2+(y/y_e)^2]$, the dispersion relation corresponding to Eq. (24) can be found in the literature as the solution of a homogeneous eigenvalue problem in the k-space if $\sigma_0\, y_e^2/(1+\widetilde{\rho}^2) \ll 1$.[25] We also note that in the appendix collisions are introduced and $y_e = x_e/x_A$ is redefined to depend on collision frequency (see Eq. (A-2)). We have developed several other approaches for solving Eq. (24)

when $\sigma_0 \ll 1$. Though σ_0 is more restrictive than Ref. (25) our method allows $g(y/y_e)$ to be arbitrary. Hence our method generalizes in some respects solutions that have previously been found. We have further compared the accuracy of the approximate solution in the literature with numerical results. We find an important case where a different form for the asymptotic solution gives more accurate results than what has been previously obtained.

The dispersion relation given in the literature for the Lorentzian conductivity model[20] in terms of our notations is

$$\Delta = \Delta_1 \equiv \frac{\pi}{8}\tilde{\sigma}^{3/2} \cdot \frac{\dfrac{\Gamma^2(\nu)}{\Gamma^2(5/4+\nu/2)} - \left(\dfrac{\tilde{\sigma}y_e^{*2}}{4}\right)^{\nu} \dfrac{\Gamma^2(-\nu)}{\Gamma^2(5/4-\nu/2)}}{\dfrac{\Gamma^2(\nu)}{\Gamma^2(-1/4+\nu/2)} - \left(\dfrac{\tilde{\sigma}y_e^{*2}}{4}\right)^{\nu} \dfrac{\Gamma^2(-\nu)}{\Gamma^2(-1/4-\nu/2)}} , \tag{25}$$

where $\tilde{\sigma} \equiv -\sigma_0/(1+\tilde{\rho}^2)$, $\nu = \sqrt{1/4+\tilde{\sigma}}$, and $y_e^{*2} = 2y_e^2/(1+\tilde{\rho}^2)$ (note that care must also be taken for the branch of the square root). In addition there is a quoted restriction $\tilde{\sigma}y_e^{*2} \ll 1$. This dispersion relation also breaks down if ν approaches a negative integer. However, as we shall see, if $\mathrm{Re}\,\nu > 1$ the condition $\tilde{\sigma}y_e^{*2} \ll 1$ does not appear to restrict the validity of Eq. (25). If $|\tilde{\sigma}| \gg 1$ (and $\mathrm{Re}\,\tilde{\sigma} > 0$), Eq. (25) becomes

$$\Delta_1 \sim \Delta_3 + \mathcal{O}\left(y_e^{*2}\sqrt{\tilde{\sigma}}\right) ,$$

with $\Delta_3 = \pi(1 + 1/4\tilde{\sigma})$, where we have used the large asymptotic expansion of the gamma function to second order. Thus under a wide variety of conditions y_e^* can be ignored in the dispersion relation if $\tilde{\sigma}$ is a moderate or large value, and $\mathrm{Re}\,\tilde{\sigma} > 0$.

The important case where y_e^* must be accounted for occurs when $\nu \to 1/2$ (or equivalently $\tilde{\sigma} \ll 1$). Then the term $1/\Gamma^2(-1/4+\nu/2)$ approaches zero and the y_e^* correction in the denominator of Eq. (25) needs to be kept. If the y_e^* term in the numerator is considered negligible, Eq. (25) can be written as

$$\Delta_1 \doteq \frac{\pi}{8}\tilde{\sigma}^{3/2} \frac{\Gamma^2(\nu)}{\left[\dfrac{\Gamma^2(\nu)}{\Gamma^2(-1/4+\nu/2)} - \left(\dfrac{\tilde{\sigma}y_e^{*2}}{4}\right)^{\nu} \dfrac{\Gamma^2(-\nu)}{\Gamma^2(-1/4-\nu/2)}\right] \Gamma^2\left(\dfrac{5}{4}+\dfrac{\nu}{2}\right)} . \tag{26}$$

One might expect that if $\tilde{\sigma}$ is moderate to large, that the dispersion relation is insensitive to y_e^*. However, for smaller $\tilde{\sigma}$, $\nu \to 1/2$ and then the y_e^* term can compete with the first term in the denominator as it vanishes as $\nu \to 1/2$. As the dependence is not expected to be important for large $\tilde{\sigma}$, we set $\nu = 1/2$ in the term containing the y_e^* dependence. This retains y_e^* term to its correct form when $\nu = 1/2$, and keeps the term small for larger $\tilde{\sigma}$. One then obtains a model dispersion relation of the form

$$\Delta = \Delta_2 \equiv \frac{\pi\tilde{\sigma}^{3/2}}{8} \frac{\Gamma^2(\nu)}{\frac{\Gamma^2(\nu)\Gamma^2\left(\frac{5}{4}+\nu/2\right)}{\Gamma^2(-1/4+\nu/2)} - \left(\frac{\sigma y_e^{*2}}{4}\right)^{\nu} \Gamma^2(3/2)} . \tag{27}$$

As we shall observe later the relation $\Delta = \Delta_2$ can be more accurate than the expression $\Delta = \Delta_1$ as y_e^* increases. Note, however, that the expression for Δ_2 is inaccurate if $\nu \to 0$, and then the y_e^* term in the numerator of Eq. (25) must be retained.

Now continuing with the small $\tilde{\sigma}$ case, we can expand Eq. (26) and find with $\nu = \sqrt{1/4+\tilde{\sigma}} \sim 1/2 + \tilde{\sigma}$, and $1/\Gamma(x) \to x$ as $x \to 0$,

$$\Delta = \Delta_4 \equiv \frac{1}{\frac{\sqrt{\tilde{\sigma}}}{2} - \frac{y_e^*}{\tilde{\sigma}\pi}\left(\frac{\tilde{\sigma} y_e^{*2}}{4}\right)^{\tilde{\sigma}}} \sim \frac{1}{\frac{\sqrt{\tilde{\sigma}}}{2} - \frac{y_e^*}{\tilde{\sigma}\pi}\left[1 + \tilde{\sigma}\,\ell n\left(\frac{\tilde{\sigma} y_e^{*2}}{4}\right)\right]} . \tag{28}$$

By rewriting Eq. (28) we find

$$\sqrt{\tilde{\sigma}} = \frac{2}{\Delta} + \frac{2y_e^*}{\tilde{\sigma}\pi}\left(1 + \tilde{\sigma}\ell n(\tilde{\sigma} y_e^{*2}) + \mathcal{O}(\tilde{\sigma})\right) . \tag{29}$$

Equation (29) is the appropriate asymptotic limit we wish to generate in the limit of small y_e^* and $\tilde{\sigma}$ when the electron kinetics are described by more complicated functions than that in the Lorentzian conductivity model.

To compare the accuracy of the various approximations for Δ, we evaluate Δ numerically and compare the result given by Δ_1 [Eq. (25)], Δ_2 [Eq. (27)], and Δ_5 (obtained from Eq. (28) neglecting the $\mathcal{O}(\tilde{\sigma}\,\ell n\,\tilde{\sigma})$ term)

$$\Delta_5 \equiv \frac{1}{\frac{\sqrt{\tilde{\sigma}}}{2} - \frac{y_e^*}{\tilde{\sigma}\pi}} . \tag{30}$$

To obtain Δ numerically we solve the equation

$$\frac{d}{dy}\frac{1}{y^2+1}\frac{d\Psi}{dy}+\frac{2\Psi}{(y^2+1)^2}-\frac{\tilde{\sigma}\Psi}{y^2+y_e^{*2}}=\frac{1}{(y^2+1)^2} \tag{31}$$

and use

$$\Delta=\pi-8\int_0^\infty dy\,\frac{\Psi(y)}{(y^2+1)^2}\,. \tag{32}$$

Equation (31) needs to be solved with the boundary condition $d\Psi/dy\Big|_{y=0}=0$, and $\Psi(y)\to Ay\exp(-\sqrt{\tilde{\sigma}}\,y)-(y^2+y_e^{*2})/y^4\tilde{\sigma}$ for $y\gg$ Max $\left\{1/\sqrt{\tilde{\sigma}},1\right\}$, and where A is a constant. In practice, Eq. (32) can be solved as a sum of a homogeneous and inhomogeneous equation; i.e. $\Psi=\Psi_I(y)+A\Psi_H(y)$ with the boundary conditions at large y being $\Psi_I(y)\to-(y^2+y_e^{*2})/y^4\tilde{\sigma}$ for the inhomogeneous equation and the equation $\Psi_H(y)=y\exp(-\sqrt{\tilde{\sigma}}\,y)$ for the homogeneous equation. The constant A is then found to be

$$A=-\Psi_I'(y=0)/\Psi_H'(y=0)\,, \tag{33}$$

where the values at $y=0$ are obtained by direct integration of the two differential equations. Then with $\Psi(y)=\Psi_I(y)+A\,\Psi_H(y)$ determined, the expression for Δ is obtained from Eq. (32). A comparison of various values of Δ^{-1} obtained from: numerical evaluations Δ_n^{-1}, Δ_2^{-1}, and Δ_4^{-1} are given in Fig. 1.

One observes that for moderate values of y_e^*, Δ_2 is more accurate than Δ_1, as the accuracy of Δ_1 is only good for very small y_e^* (as $\tilde{\sigma}$ increases, the smaller y_e^* needs to be for accuracy) while Δ_2 is accurate for $y_e^*\lesssim 1$. Of course Δ_5 is inaccurate when $\tilde{\sigma}$ is not small. We actually find in results to be presented elsewhere, that the use of Δ_1 to describe kink mode for reasonable physical parameters leads to a distortion of the mode spectrum, whereas Δ_2 and Δ_5 given accurate representations of the spectrum. However, the applicability of Eq. (27), when the parameters are complex, needs further verification, particularly as Δ_2 is a fitting formula rather than an asymptotic formula.

Now, we study the solutions in the small $\tilde{\sigma}$ limit for a general electron conductivity model.

It is interesting to note that $\Psi = \alpha + y$ (with $\alpha = -2/\Delta$) is an exact solution of Eq. (23) for $\sigma_0 = 0$. However, this solution does not satisfy the boundary condition either at $y = 0$, or at $y \to \infty$. Therefore, the inclusion of the finite contribution of σ_0, even if it is small, is essential for the existence of a mode. Taking into account the small σ_0 contribution, we can obtain the asymptotic solution of Eq. (23) in small y-limit from the following equation

$$\frac{d^2\Psi}{dy^2} + \sigma_0 \frac{g(y/y_e)}{y^2\left[1 + \tilde{\rho}^2 g(y/y_e)\right]} \Psi = c_0 \ , \tag{34}$$

where

$$c_0 \equiv -\frac{8}{\Delta - \pi} \int_0^\infty dy \, \frac{\Psi(y)}{(y^2+1)^2} \ . \tag{35}$$

The first integration of Eq. (26) yields

$$\frac{d}{dy}\Psi = -\sigma_0 \int_0^y dy \, \frac{g(y/y_e)}{y^2\left[1 + \tilde{\rho}^2 g(y/y_e)\right]} \Psi + c_0 y \ , \tag{36}$$

which satisfies the boundary condition at $y = 0$. Now writing .

$$\Psi = \alpha + \delta\Psi \tag{37}$$

we find

$$\frac{d}{dy}\delta\Psi = -\sigma_0 \alpha \int_0^\infty dy \, \frac{g(y/y_e)}{y^2\left[1 + \tilde{\rho}^2 g(y/y_e)\right]} \tag{38}$$

for $y \gg y_e$ (but $y < 1$). We then have $\delta\Psi$ proportional to y as in the limit $\sigma_0 = 0$, with α determined to be

$$\alpha = -\frac{1}{\sigma_0 \int_0^\infty dy \, \frac{g(y/y_e)}{y^2\left[1 + \tilde{\rho}^2 g(y/y_e)\right]}} \ . \tag{39}$$

For the Lorentzian conductivity model in Appendix A (Eqs. (A1), (A2)) we find that

$$\alpha = \frac{2y_e^*}{\pi\tilde{\sigma}} \tag{40}$$

with

$$y_e^{*2} \equiv \frac{2y_e^2}{1+\widetilde{\rho}^2} \,. \tag{41}$$

More generally, it is then convenient to define $\widehat{y}_e^*$ as

$$\frac{1}{\widehat{y}_e^*} \equiv \frac{2(1+\widetilde{\rho}^2)}{\pi} \int_0^\infty dy \, \frac{g(y/y_e)}{y^2\,[1+\widetilde{\rho}^2 g(y/y_e)]} \tag{42}$$

Then Eq. (39) is written as

$$\alpha = \frac{2\widehat{y}_e^*}{\pi\widetilde{\sigma}} \,. \tag{43}$$

We note that for small, but finite σ_0, the test function $\Psi = \alpha + y$ nearly satisfies the differential equation over a large domain ($y \ll 1/\sqrt{\widetilde{\sigma}}$ except $y \sim \widehat{y}_e^*$) with $\alpha = -\frac{2}{\Delta}$. Then we can write a dispersion relation as

$$\alpha + \frac{2}{\Delta} = \mathcal{O}(\sqrt{\widetilde{\sigma}}\,) \tag{44}$$

with α given by Eq. (43). The right-hand side of Eq. (44), $\mathcal{O}(\sqrt{\widetilde{\sigma}}\,)$, is unimportant for small but finite $\widetilde{\sigma}$. The contribution from $\mathcal{O}(\sqrt{\widetilde{\sigma}}\,)$ to the dispersion relation can be important only if α becomes so small that it is at the same order as $\mathcal{O}(\sqrt{\widetilde{\sigma}}\,)$. To include this case we use a more general test function

$$\Psi_t = \alpha + y \, \exp\left[-\sqrt{\widetilde{\sigma}}\, y\right] \tag{45}$$

with α given by Eq. (43), to calculate the quadratic form Eq. (24) to the linear order in $\sqrt{\widetilde{\sigma}}$. The form $y\exp(-\sqrt{\widetilde{\sigma}}\, y)$ is chosen as it is a solution to the homogeneous equation of Eq. (23) for $y \gg y_e$. The various integrals in the quadratic form are found to be

$$\int_0^\infty dy \left[\frac{(d\Psi_t/dy)^2}{y^2+1} - \frac{2\Psi_t^2}{(y^2+1)^2}\right] \approx -\frac{\pi}{2}\,\alpha^2 - 4\alpha\left(\frac{1}{2} - \frac{\pi}{4}\sqrt{\widetilde{\sigma}}\right) \tag{46}$$

$$\int_0^\infty dy \, \frac{\Psi_t(y)}{(y^2+1)^2} = \frac{1}{2}\left(1+\frac{\pi}{2}\,\alpha\right) - \frac{\pi}{4}\sqrt{\widetilde{\sigma}} + \mathcal{O}(\widetilde{\sigma}\,\ell n\,\widetilde{\sigma}) \tag{47}$$

$$\int_0^\infty dy \, \frac{g(y/y_e)\Psi_t^2}{y^2\,[1+\widetilde{\rho}^2 g(y/y_e)]} = \frac{\alpha^2\pi}{2(1+\widetilde{\rho}^2)y_e^*} + \frac{1}{2(1+\widetilde{\rho}^2)\sqrt{\widetilde{\sigma}}} + 2\alpha\ell n(1/\sqrt{\widetilde{\sigma}}y_e^*) \,. \tag{48}$$

In the calculation of the left-hand side of Eq. (49) we have used the asymptotic form

$$\frac{g(y/y_e)}{1+\widetilde{\rho}^2 g(y/y_e)} \longrightarrow \begin{cases} \dfrac{1}{1+\widetilde{\rho}^2} & y \gg y_e \\ \dfrac{y^2}{(1+\widetilde{\rho}^2)y^2+2y_e^2} & y \ll y_e \end{cases}$$

and ignored the term at the order $y_e^* \ell n\, y_e^* \ll 1$. Substituting Eqs. (46)–(48) into the quadratic form Eq. (24), we obtain a dispersion relation

$$\alpha + \frac{2}{\Delta} = \frac{\sqrt{\widetilde{\sigma}}}{1+\frac{\pi}{2}\alpha} \,. \tag{49}$$

In Eq. (49) if $\alpha \gtrsim \mathcal{O}(1)$, the right-hand side of Eq. (49) is ignorable compared to α. If $\alpha \sim \mathcal{O}(\sqrt{\widetilde{\sigma}})$, the α-dependence on the right-hand side of Eq. (49) can be ignored, as is consistent with our derivation, in which only terms of linear order of $\sqrt{\sigma}$ are retained. We note that if this α-dependence were not ignored, we geneate a fictitious root, $1+\pi\alpha/2 \sim 0$, which violates the condition of Eq. (44). Correct to $\sqrt{\widetilde{\sigma}}$ order the dispersion relation becomes

$$\alpha + \frac{2}{\Delta} = \sqrt{\widetilde{\sigma}} \,. \tag{50}$$

Equation (50) is the same as that obtained from direct solution of the eigenmode equation given in Appendix A [Eq. (A14) with x_e^* is replaced by $\hat{x}_e^*$ defined by Eq. (A19)].

IV. Analysis of Dispersion Relation and Numerical Results

For clarity we first analyze basic properties of the dispersion relation given by Eq. (50) in the Lorentzian conductivity model (see the appendix where all quantities are defined). The dispersion relation can be written as

$$D(\widetilde{\omega}; \delta\widetilde{W}, k_0, \tau) \equiv \widetilde{\omega}(\widetilde{\omega}-1) - \delta\widetilde{W}\, d(\omega) + \frac{i d^2(\widetilde{\omega}) k_0 (\widetilde{\omega}+i\widetilde{\nu})^{1/2}}{\widetilde{\omega}^{1/2}(\widetilde{\omega}-1)^{1/2}(\widetilde{\omega}+\tau)^{1/2}} = 0 \tag{51}$$

with $\delta\widetilde{W} = \frac{\sqrt{2}}{\pi}\frac{\delta\widehat{W}_c\,\overline{\rho}^2}{\widehat{\rho}_i}$, $\widetilde{\omega} = \omega/\omega_i^*$, $\overline{\rho} = \widehat{\rho}_i\omega_A/\omega_i^* = 2L_n/\beta_i^{1/2}\,L_s$, β_i is the ion beta, L_n the density scale length, $d(\widetilde{\omega}) = [\widetilde{\omega}(1+\tau)/(\widetilde{\omega}+\tau)]^{1/2}$, $k_0 = \left(\frac{m_e}{m_i}\right)^{1/2} S^3/\pi\,\beta_i^2$, $S = 2L_n/L_s$, $\tau = T_e/T_i$, and $\widetilde{\nu} = \nu_{ei}/\omega_i^*$. The self-consistency condition for the accuracy of Eq. (51) requires $|x_e^{*2}/x_A^2| = |2m_e(1+i\widetilde{\nu})/m_i\,\beta_i(1+\tau)| \ll 1$, and $|\overline{\sigma}| = |2(\widetilde{\omega}-1)(\widetilde{\omega}+\tau)/(1+\tau)\overline{\rho}^2| \ll 1$. Note that the natural parameters for our analysis, treating $\tau \approx 1$ and $\widetilde{\nu} \approx 1$, $\overline{\rho}^{-2} = L_s^2\,\beta_i/4L_n^2 \ll 1$ and $2m_e/m_i\,\beta_i \ll 1$. This defines a β_i interval for the validity of the analysis given by $\frac{2m_e}{m_i} \ll \beta_i \ll 4L_n^2/L_s^2$. We note only the branches that are physically compatible with causality should be chosen in Eq. (5). In this case the branch cuts of the square root in Eq. (51) should be chosen so that the function $[\widetilde{\omega}(\widetilde{\omega}-1)]^{1/2}$ is in the first or second quadrant if $\mathrm{Im}\,\widetilde{\omega} > 0$. We choose the branch that is the analytical continuation of $[\widetilde{\omega}(\widetilde{\omega}-1)]^{1/2}$ when $\mathrm{Im}\,\widetilde{\omega}$ changes sign.

It is instructive to determine the total roots satisfying causality by examining the limiting case of $\delta\widetilde{W} = \tau = \widetilde{\nu} = 0$. In this limit Eq. (51) becomes

$$\widetilde{\omega}(\widetilde{\omega}-1) + \frac{ik_0}{\sqrt{\widetilde{\omega}(\widetilde{\omega}-1)}} = 0\ . \tag{52}$$

Assuming $k_0 \ll 1$, we can solve this equation perturbatively. Near $\widetilde{\omega} = 1$ we have only two roots satisfying causality. One is a zero growth rate root with $\widetilde{\omega} = 1 - k_0^{2/3}$, the other is a stable root with $\widetilde{\omega} = 1 + k_0^{2/3}\exp(-i\pi/3)$. We also have solutions of low frequency modes. In the ion direction there is a zero growth rate root, $\widetilde{\omega} = k_0^{2/3}$; and a stable root $\widetilde{\omega} = -k_0^{2/3}\exp(i\pi/3)$ in the electron direction. The two zero growth rate modes in the small k_0 limit turn out to be a pair of conjugate MHD-like modes for finite k_0, $\widetilde{\omega}_\pm = (1 + \sqrt{1-4k_0^{2/3}})/2$, which are the solutions of the following equation

$$\widetilde{\omega}(\widetilde{\omega}-1) = -k_0^{2/3}\ . \tag{53}$$

This dispersion relation explicitly describes the coupling between the positive energy wave ($\widetilde{\omega} > 1/2$) and the negative energy wave ($\widetilde{\omega} < 1/2$) due to the coupling constant $k_0^{2/3}$ arising

from magnetic shear. Altogether, there are four modes satisfying causality: two of them are MHD-like with zero growth in the small k_0 limit; the other two are of drift type, which, for finite k_0, become

$$\tilde{\omega}^{(\pm)} = \left(1 \pm \sqrt{(1 + 4k_0^{2/3} \exp(\mp i\pi/3)}\right) \Big/ 2 \ ,$$

where $\tilde{\omega}^{(+)}$ and $\tilde{\omega}^{(-)}$ refers to the mode in the ion, and electron direction respectively. These may be related to the stable modes analyzed in Ref. 26–28.

The reduced dispersion relation for the conjugate modes, Eq. (53), can be generalized to include finite $\delta\widetilde{W}$ as

$$\tilde{\omega}(\tilde{\omega} - 1) = -k^{2/3} \ , \tag{54}$$

where $k^{1/3}$ is the positive real root of the following cubic equation

$$k + \delta\widetilde{W}\, k^{1/3} - k_0 = 0 \ . \tag{55}$$

Equation (55) yields the conditions when the contribution to the coupling constant k from the MHD free energy (negative $\delta\widehat{W}_c$) is more important than that from magnetic shear. This condition is estimated as $\delta\widetilde{W}/k_0^{2/3} > 1$, and in terms of physical quantities, as

$$-\delta\widehat{W}_c > \hat{\rho}_i (m_e\pi/m_i\,\beta_i)^{1/3} \ . \tag{56}$$

This condition is typically not satisfied if $\delta\widehat{W}_c$ is estimated by the Bussac formula, Eq. (9), for typical parameters in tokamak discharges, e.g. $\delta\widehat{W}_c \approx 10^{-3}$ from the Bussac formula, whereas $\tilde{\rho}_i(\frac{m_e\pi}{m_i\,\beta_i})^{1/3} \approx 10^{-2}$. Consequently, the most important driving force inherent to the kink instability seems to be the parameter k_0 which is proportional to the local shear. Note that the condition for the unstable mode to be insensitive to $\delta\widehat{W}_c$ is a condition independent of the local shear. One can also readily verify that the scaling given by Eq. (56) holds for $\tau \approx 1$ and $\tilde{\nu} \gtrsim 1$.

To analyze the stability limits of Eq. (51) we first assume $\tilde{\nu} = 0$. We then observe that $D(\tilde{\omega})$ is real for real $\tilde{\omega}$ if $0 < \tilde{\omega} < 1$. Marginal stability arises in this interval if two

roots coalesce, which is equivalent to the condition $\partial D/\partial\tilde{\omega} = 0$. For a given τ one can then determine the relation at marginal stability between the two parameters k_0 and $\delta\widetilde{W}$ by simultaneously solving $D(\tilde{\omega}) = \partial D(\tilde{\omega})/\partial\tilde{\omega} = 0$. This condition shall be referred to as the "reactive" marginal stability condition. For $\tau \ll 1$ and $\tau \gg 1$ the relation is obtained analytically. For $\tau \ll 1$, $d(\tilde{\omega}) \to 1$ and then $D(\tilde{\omega})$ depends only on $\Omega \equiv \tilde{\omega}(\tilde{\omega}-1)$. Then $\partial D/\partial\tilde{\omega} = \dfrac{\partial D}{\partial\Omega}\dfrac{\partial\Omega}{\partial\tilde{\omega}} = \dfrac{\partial D}{\partial\Omega}(2\tilde{\omega}-1)$. Thus, $\tilde{\omega} = 1/2$ is a marginal point, and then from $D(\tilde{\omega}=1/2) = 0$ we find that marginal stability occurs when

$$\delta\widetilde{W} = -1/4 + 2k_0\ , \qquad \text{while stability requires}$$

$$\delta\widetilde{W} > -1/4 + \frac{2}{\pi}\left(\frac{m_e}{m_i}\right)^{1/2}\frac{S^3}{\beta_i^2}\ . \tag{57}$$

The last term in Eq. (57) is an intrinsically destabilizing term. If the second term is large, MHD instability arises even when $\delta\widetilde{W} > 0$. We also note even if the last term in Eq. (57) were not important, the stabilization condition is different from that in previous studies[12–18] that neglected the strong Larmor radius effects which would be valid if $\overline{\rho} \ll 1$. For example, the dispersion relation in Ref. 13–18 has as the dispersion relation, assuming $\delta\widetilde{W} < 0$,

$$\tilde{\omega}(\tilde{\omega}-1) + \delta\widetilde{W}^2\frac{\pi^2}{2\overline{\rho}^2} = 0$$

with the stability condition $-\delta\widetilde{W} < \sqrt{2\pi}\,\overline{\rho}$. This condition is more optimistic than it should be when $\overline{\rho} \gg 1$ as can be seen by comparing with Eq. (57), even with the last term neglected.

If $\tau \neq 0$, the determination of marginal stability is more difficult. The simultaneous solution of $D(\tilde{\omega}) = 0$ and $\dfrac{\partial D(\tilde{\omega})}{\partial\tilde{\omega}} = 0$ is readily performed numerically and shows in Fig. 2a, where a plot of $\delta\widetilde{W}$ vs. k_0 is given for various parameters of τ. In Fig. 2b the marginal frequency is given as a function of k_0.

The plots in Fig. 1a show two branches to the marginal stability curve if $\tau < 1$. If $1/8 < \tau < 1$, these two branches are connected at a cusp point where three roots coalesce; i.e. where $\partial^2 D/\partial\omega^2 = 0$. The upper branch terminates at a finite k_0 where $\tilde{\omega} = 0$ and

$\delta\widetilde{W} = 0$. For $\tau < 1/8$ the marginal stability boundary extends to arbitrarily $\delta\widetilde{W}$ as k_0 gets arbitrarily large.

The lower branch can be interpreted as the marginal boundary for MHD instability. Starting from a point on this branch, one goes in the unstable region by decreasing $\delta\widetilde{W}$, for a given k_0. This root blends into the standard MHD growth rate. Increasing $\delta\widetilde{W}$ from the lower stability boundary brings one into a stable region. However, for $\tau < 1$, increasing $\delta\widetilde{W}$ further causes the intersection with the upper stability boundary, and the mode destabilizes when $\delta\widetilde{W}$ lies above this boundary.

There is still the "dissipative" stability boundary to consider, which is obtained by simultaneously solving Re $D(\omega)$ = Im $D(\omega) = 0$. Note that the second reactive stability boundary merges with the dissipative stability boundary when $\delta\widetilde{W} = \tilde{\omega} = 0$, which occurs when $k_0 = \dfrac{\tau^{3/2}}{1+\tau} \equiv k_{0c}$. If $\tau < 1$, it can be shown that the instablity region occurs for $k < k_{0c}$ and $\delta\widetilde{W} > 0$. At marginal stability the frequency of the mode satisfies the condition

$$k_0 = \frac{(1-\tilde{\omega})^{2/3}(\tilde{\omega}+\tau)^{3/2}}{1+\tau} \equiv F(\omega) \; . \tag{58}$$

For $\tau < 1$, as k_0 decreases from k_{0c}, ω decreases from $\tilde{\omega} = 0^-$ to $\tilde{\omega} \to -\tau$ as $k_0 \to 0$. Asymptotically we find

$$\tilde{\omega} \longrightarrow \begin{cases} -\dfrac{3}{2}\,(k_{0c} - k_0)\,\dfrac{1-\tau}{1+\tau} \; , & k_0 \doteq k_{0c} \\ -\tau + [k_0(1+\tau)]^{2/3} \; , & k_0 \ll k_{0c} \; . \end{cases}$$

The dissipative instability region can be thought of as an ω_e^* mode that is destabilized by positive MHD energy.

For $\tau > 1$, there is only one reactive stability boundary. It terminates at the dissipative instability boundary at $\delta\widetilde{W} = 0$ and $k_0 = k_{0c} \equiv \tau^{3/2}/(1+\tau)$. The dissipative boundary now exists for $\delta\widetilde{W} = 0$ and

$$k_{0c} < k_0 < k_{\max} \equiv (1+\tau)^2/8$$

and in the frequency range

$$\omega_{c1} \equiv -\frac{(\tau - 1)}{2} < \omega < 0 \,.$$

The instability region is now $\delta\widetilde{W} < 0$. One also finds that the marginal stability curve has another branch for $-\tau < \omega < \omega_{c1}$ and $k < k_{\max}$. In this branch $\delta W_c > 0$ corresponds to the instability region as in the case $\tau < 1$.

Altogether we see a relatively small stability region determined by Eq. (51). In Fig. 3 we indicate schematically by the hatched area the stable region for various τ for $\delta\widetilde{W}$ near zero and $k_{0c} < k < k_{\max}$, there are two different marginal modes, one of which is unstable for $\delta\widetilde{W} > 0$ and the other for $\delta\widetilde{W} < 0$. For $k > k_{\max}$ there is instability at $\delta\widetilde{W} = 0$ and the unstable mode is the same for either sign of $\delta\widetilde{W}$.

We also note that when $\delta\widetilde{W}$ is greater than the critical $\delta\widetilde{W}$ for reactive stability (the critical $\delta\widetilde{W}$ can be determined from the plot in Fig. 1a) that there are two real frequency modes with $\tilde{\omega} < 1$, the positive energy mode where $\tilde{\omega}$ is greater than the critical frequency at marginal stability (the frequency of the marginal mode is plotted in Fig. 1b), and the negative energy mode at frequency less than the frequency at marginal stability. When electron collisional effects are introduced, the negative energy wave becomes unstable. This destabilization is illustrated in Fig. 4 for a particular set of physical parameters. Note, that now a well-defined stability threshold disappears, as the negative energy wave, that was destabilized, blends into MHD unstable mode as S, the shear parameter increases. We also note that the unstable negative wave goes to very low frequency for small S. In this case stability effects due to ion drift resonances arise that have not been taken into account in our theory.

A more realistic electron dynamics model when $\tilde{\nu} \ll 1$ should take into account electron Landau damping which gives rise to positive dissipation. This dissipation is not contained in the Lorentz conductivity model. Hence even as $\tilde{\nu} \to 0$ there can be appreciable destabiliza-

tion of the negative energy wave. In the collisionless limit we have also taken into account the effect of η_e. In Fig. 5 numerical results for the real and imaginary frequencies are given for a particular set of parameters. Note that in this figure appreciable growth rates are now present below $S < .15$ (where the Lorentzian model with $\tilde{\nu} = 0$ gives stability). Also note that as η_e increases the growth rates decrease, as the positive energy dissipation due to finite η_e decreases.

For the above numerical results we find that one of the self-consistent conditions, $(x_e^*/x_A^2) \ll 1$ is well satisfied for $\beta_i > .5\%$. However, the other self-consistent condition, $\bar{\sigma} \ll 1$, is only barely satisfied. Typically, $\bar{\sigma}$ ranges from .3 to .4. For a more accurate investigation one should take into account the contribution from $\bar{\sigma} \sim \mathcal{O}(1)$. As we have noted in Sec. III, a relatively complicated analytic dispersion relation has been determined in Ref. 20. However, when $\tilde{\sigma} \approx 1$, a simple description of the electron kinetic effects is not as easily attained.

V. Conclusion

We have shown how to analyze with simple functions the $m = 1$ kink mode in the parameter regime $\frac{m_e}{m_i} \ll \beta_i \ll L_n^2/L_s^2$ and when $\nu_e/\omega \approx 1$. In this case the layer width is comparable to the ion Larmor radius. A relatively simple dispersion relation has been derived from which concrete stability criteria have been obtained. The most striking aspect of the dispersion relation is a strong sensitivity to local magnetic shear and local density gradients. These quantities appear more important than the MHD energy in determining stability and growth rates for the modes where $\omega/\omega_i^* > 0$. It is conceivable that these local quantities at the $q = 1$ surface are important in understanding experimentally puzzling sawteeth phenomena.

Appendix A — Derivation of Dispersion Relation from Direct Solution of Eigenmode Equation

The derivation is split into two steps. We first obtain the dispersion relation for the Lorentzian conductivity model, and then we extend the derivation to the general conductivity model given by Eqs. (5) and (6).

For the Lorentzian conductivity model we take $\sigma(x)$ to be of the following form

$$\sigma(x) = \sigma_0 \frac{x^2}{2x_r^2 - x^2} \ , \tag{A1}$$

where σ_0 is defined after Eq. (5) and collisionality can be described if x_r^2 has the form

$$x_r^2 = \omega(\omega + i\nu_{ei})/(k_{||}' v_e)^2 \ . \tag{A2}$$

This conductivity model is obtained from a simple fluid description that includes electron-ion drag and an isothermal electron pressure. This model gives qualitatively similar results as more rigorous derivations in the large and small ν_{ei}/ω limits. We now rewrite Eq. (2) in the following way,

$$\frac{d}{dx}\frac{x^2}{x^2 - x_A^2}\frac{d}{dx}\left(\frac{\Psi}{x}\right) + \frac{\overline{\sigma}}{x_A^2\left(\frac{x_e^{*2}}{x^2} - 1\right)}\left(\frac{\Psi}{x}\right) = \frac{2x}{(x^2 - x_A^2)^2}\Psi_0 \ , \tag{A3}$$

where

$$\Psi_0 \equiv -\frac{4x_A^2}{\Delta' + \frac{i\pi}{x_A}} \int_0^\infty dx \, \frac{\Psi(x)}{(x^2 - x_A^2)^2} \tag{A4}$$

and

$$1 + \frac{\widehat{\rho}_i^2 \sigma_0}{2x_A^2} = \frac{(1 + 1/\tau)\widetilde{\omega}}{\widetilde{\omega} - 1} \ , \quad \overline{\sigma} \equiv \frac{\sigma_0}{1 + \frac{\widehat{\rho}_i^2 \sigma_0}{2x_A^2}} = \frac{2(\widetilde{\omega} - 1)(\widetilde{\omega} + \tau)}{(1 + \tau)\,\overline{\rho}^2}$$

$$\overline{\rho}^2 = \frac{4L_n^2}{L_s^2\,\beta_i} \ , \qquad x_e^{*2} \equiv \frac{2x_r^2}{1 + \frac{\widehat{\rho}_i^2 \sigma_0}{2x_A^2}} = \frac{2m_e(\widetilde{\omega} + i\widetilde{\nu})(\widetilde{\omega} - 1)\omega_i^{*2}}{m_i\,\beta_i(1 + \tau)\omega_A^2} \ .$$

Provided $(x_e^*/x_A)^2 \approx \dfrac{m_e}{\tau m_i \beta_i} \ll 1$, we can first solve Eq. (A3) in the region, where $x^2 \ll x_A^2$ (region I) and then in the region, where $x^2 \gg x_e^{*2}$ (region II) separately.

For $x^2 \ll x_A^2$ Eq. (A3) reduces to

$$\frac{d^2\Psi^{(I)}(x)}{dx^2} + \frac{\overline{\sigma}}{x^2 - x_e^{*2}}\,\Psi^{(I)}(x) = -\frac{2\Psi_0}{x_A^2}\,. \tag{A5}$$

The solution of Eq. (A5), satisfying the boundary condition at $x = 0$, $d\Psi^{(I)}/dx\Big|_{x=0} = 0$, is

$$\Psi^{(I)}(x) = \left\{ c\,F\left(-\frac{1}{4} + \frac{\nu}{2}\,,\; -\frac{1}{4} - \frac{\nu}{2}\,,\; \frac{1}{2}\,;\; \frac{x^2}{x_e^{*2}}\right) - \frac{2}{2+\overline{\sigma}} \cdot \frac{x^2 - x_e^{*2}}{x_A^2} \right\} \Psi_0\,, \tag{A6}$$

where $F(\alpha, \beta, \gamma; z)$ is the hypergeometric function, $\nu \equiv \sqrt{1/4 - \overline{\sigma}}$, and c is a constant to be determined.

For $x^2 \gg x_e^{*2}$ Eq. (A3) reduces to

$$\frac{d}{dx}\,\frac{x^2}{x^2 - x_A^2}\,\frac{d}{dx}\left(\frac{\Psi^{(II)}}{x}\right) - \frac{\overline{\sigma}}{x_A^2}\left(\frac{\Psi^{(II)}}{x}\right) = \frac{2x}{(x^2 - x_A^2)^2}\,\Psi_0\,. \tag{A7}$$

The solution of Eq. (A7), satisfying the boundary condition at infinity, $\Psi^{(II)}(x \to \infty) = 0$, is

$$\Psi^{(II)}(x) = -\frac{\Psi_0}{\sqrt{\overline{\sigma}}\,x_A}\,x \Bigg\{ \left(\frac{I_\nu(z)}{2\sqrt{z}} + \sqrt{z}\,\frac{dI_\nu(z)}{dz}\right) \int_\infty^z dz'\,\sqrt{z'}\,K_\nu(z') \\ - \left(\frac{K_\nu(z')}{2\sqrt{z}} + \sqrt{z}\,\frac{dK_\nu(z)}{dz}\right) \left(\int_0^z dz'\,\sqrt{z'}\,I_\nu(z') + \bar{c}\right) \Bigg\}\,, \tag{A8}$$

where $I_\nu(z)$ and $K_\nu(z)$ are modified Bessel functions, $z \equiv \sqrt{\overline{\sigma}}\,x/x_A$, and $\bar{c}$ is another constant to be determined.

To match $\Psi^{(I)}(x)$ in the overlapping region ($x_e^* \ll x \ll x_A$), we ought to analytically continue the hypergeometric function in Eq. (A4) into the large argument region ($x^2/x_e^{*2} \gg 1$), and then make expansion. Also, we calculate $\Psi^{(II)}(x)$ in the small z limit. Then both c and $\bar{c}$ can be determined by the matching. The expression for c and $\bar{c}$ are complicated if $\overline{\sigma}$

is not much smaller than 1/4. However, if $\sqrt{\overline{\sigma}} \ll 1$, we have simple expressions for c and $\bar{c}$,

$$c = \sqrt{\frac{\pi}{2}}\,\bar{c} = \frac{2ix_e^*}{\pi\overline{\sigma}^{3/2}\,x_A + 2ix_e^*}\ . \tag{A9}$$

To obtain dispersion relation we need to substitute the inhomogeneous solution of Eq. (A6) into Eq. (A4), and perform the integration. This is done in the small $\overline{\sigma}$ limit, whereupon $\Psi^{(II)}(x)$ in the limit $\sqrt{\overline{\sigma}}\,x/x_A \ll 1$ is approximated by

$$\Psi^{(II)}_{\rm asy}(x) = \Psi_0\left\{\sqrt{\frac{\pi}{2}}\,\bar{c} + \left(1 - \sqrt{\frac{\pi}{2}}\,\bar{c}\right)\frac{x}{\sqrt{\overline{\sigma}}\,x_A} - \left(1 - \sqrt{\frac{\pi}{2}}\,\bar{c}\right)\frac{x^2}{x_A^2}\right\} \tag{A10}$$

$$(\text{for} \qquad \sqrt{\overline{\sigma}}\,x/x_A \ll 1)\ .$$

In the small $\sqrt{\overline{\sigma}}$ limit the validity of Eq. (A10) extends to the region, where $x \gg x_A$, and the contribution to the dispersion relation in evaluating Ψ_0 at large x ($\gg x_A$) is small because of the convergence obtained from the denominator of the integrand of Eq. (A4).

Now, we show that the asymptotic form in region II, Eq. (A10), can also be effectively extended to region I, and no significant changes in the dispersion relation occur if a more accurate form of $\Psi^{(I)}(x)$ were used. To show this we study the integral required by Eq. (A7)

$$D(u) \equiv \int_0^u dx\,\frac{\Psi^{(I)}(x)}{(x^2 - x_A^2)^2}\ , \tag{A11}$$

where $\Psi^{(I)}(x)$ is given by Eq. (A6), and $x_e^{*2} \ll u^2 \ll x_A^2$. The direct integration yields

$$D(u) = \frac{1}{x_A^4}\,\Psi_0\left\{\sqrt{\frac{\pi}{2}}\,\bar{c}\,u\,F\left(-\frac{1}{4} + \frac{\nu}{2}\ ,\ -\frac{1}{4} - \frac{\nu}{2}\ ,\ \frac{3}{2}\ ;\ \frac{u^2}{x_e^{*2}}\right)\right.$$

$$\left. + \mathcal{O}(u^3/x_A^3)\right\} \xrightarrow{u \gg x_e^*} \frac{1}{x_A^4}\,\Psi_0\left\{\sqrt{\frac{\pi}{2}}\,\bar{c}\,u\left(1 - \frac{i\pi\overline{\sigma}}{4x_e^*}\,u\right) + \mathcal{O}(u^3/x_A^3)\right\}\ . \tag{A12}$$

At this stage we can introduce the effective $\Psi^{(I)}(x)$ as

$$\Psi^{(I)}_{\rm eff}(x) = \Psi_0\left\{\sqrt{\frac{\pi}{2}}\,\bar{c}\,\left(1 - \frac{i\pi\overline{\sigma}}{2x_e^*}\,x\right) + \mathcal{O}\left(\frac{x^2}{x_A^2}\right)\right\}\ , \tag{A13}$$

which yields the same $D(u)$ given by Eq. (A13), and is the same as Eq. (A12) correct to linear order. Therefore, we can use Eq. (A10) as an extended form to be substituted into Eq. (A4) and obtain the dispersion relation

$$\frac{2}{\Delta' x_A} = \frac{2ix_e^*}{\pi\overline{\sigma}x_A} + \sqrt{\overline{\sigma}}\,, \tag{A14}$$

essentially the same result as obtained in the text given by Eq. (50). It is noticeable that the detailed structure of the mode at $x \sim x_e^*$ is not important to the dispersion relation, although $\Psi(x)$ changes rapidly at $x \sim x_e^*$ as

$$\frac{d}{dx}\Psi(x)\Big|_{x\sim x_e^*} = -\Psi_0\sqrt{\frac{\pi}{2}}\,\overline{c}\,\frac{\overline{\sigma}}{2x_e^*}\,\ell n\left(1-\frac{x^2}{x_e^{*2}}\right)\,. \tag{A15}$$

The dispersion relation, Eq. (A14), is also the same as the dispersion relation obtained by other authors in the Fourier representation, for example, Eq. (18) of Ref. 25.

The above analysis indicates that the mode structure in a large domain ($x \ll x_A/\sqrt{\overline{\sigma}}$) can be approximated by a constant term plus a linar term. This is instructive to extend the Lorentzian conductivity model to the general conductivity model given by Eqs. (A1) and (A3). Since the general conductivity model is the same as the Lorentzian model in region II, we only consider the modification in region I. Instead of Eq. (A5), the eigenmode equation Eq. (20) in region I for the general conductivity model is

$$\frac{d^2\Psi^{(I)}}{dx^2} - \frac{\sigma(x)}{x^2\left[1-\dfrac{\widehat{\rho}_i^2\sigma(x)}{2x_A^2}\right]}\Psi^{(I)}(x) = -\frac{2\Psi_0}{x_A^2}\,. \tag{A16}$$

The first integration of Eq. (A16) yields

$$\frac{d\Psi^{(I)}}{dx} = -\frac{2\Psi_0}{x_A^2}\,x + \int_0^x dx\,\frac{\sigma(x)}{x^2\left[1-\dfrac{\widehat{\rho}_i^2\sigma(x)}{2x_A^2}\right]}\Psi^{(I)}(x) \tag{A17}$$

which satisfy the boundary condition at $x = 0$. To the leading order $\Psi^{(I)}(x)$ in the integral of Eq. (A17) can be replaced by $\Psi_0\sqrt{\pi/2}\,\overline{c}$ [Eq. (A13)], and the matching of $\Psi^{(I)}$ and $\Psi^{(II)}$

in the overlapping region yields

$$\sqrt{\frac{\pi}{2}}\,\bar{c}\int_0^\infty dx\,\frac{\sigma(x)}{x^2\left[1-\dfrac{\widehat{\rho}_i^2\sigma(x)}{2x_A^2}\right]}=\frac{1}{\sqrt{\overline{\sigma}}\,x_A}\left(1-\sqrt{\frac{\pi}{2}}\,\bar{c}\right)\ . \tag{A18}$$

Therefore, the modification due to general conductivity model is merely a redefinition of x_e^*, i.e.,

$$x_e^*\rightarrow\widehat{x}_e^*\equiv\frac{\overline{\sigma}}{\dfrac{2i}{\pi}\displaystyle\int_0^\infty dx\,\frac{\sigma(x)}{x^2\left[1-\dfrac{\widehat{\rho}_i^2\sigma(x)}{2x_A^2}\right]}} \tag{A19}$$

in the dispersion relation given by Eq. (A14). Obviously, $\widehat{x}_e^*$ goes back to x_e^* when $\sigma(x)$ is given by the Lorentzian model, Eq. (A1), on the right-hand side of Eq. (A19). We emphasize that the replacement of Eq. (A19) is strictly limited in the small $\overline{\sigma}$ approximation. If $\overline{\sigma}$ is order unity, the mode behavior in the overlapping region ($x_e^*\ll x\ll x_A^2$) becomes

$$\Psi(x)\sim c_1\,x^{\frac{1}{2}-\nu}+c_2\,x^{\frac{1}{2}+\nu}\ .$$

Thus, the above argument for the effective x_e^* in the kinetic electron conductivity is no longer valid.

References

1. M.N. Bussac, R. Pellat, D. Edery, and J.L. Soule, Phys. Rev. Lett. **35**, 1638 (1975).

2. L.E. Zakharov, Sov. J. Plasma Phys. **4**, 503 (1978).

3. B. Coppi, R. Galvão, R. Pellat, M.N. Rosenbluth, and P.H. Rutherford, Fiz. Plazmy **2**, 961 (1976); Sov. J. Plasma Phys. **2**, 533 (1976).

4. G. Ara, B. Basu, B. Coppi, G. Laval, M.N. Rosenbluth, and B.V. Waddell, Annals of Phys. **112**, 443 (1978).

5. PDX Group, Phys. Rev. Lett. **50**, 891 (1983).

6. Doublet-III Group, in *Heating in Toroidal Plasmas,* (Proc. 4th Int. Symp., Rome, 1984), Vol. 1, ENEA, Rome (1984), p. 21.

7. JET Team, in *Plasma Phys and Controlled Nuclear Fusion Research, 1986* (Proc. 11th Int. Conf., Kyoto, 1986), Vol. 1, IAEA, Vienna (1987) p. 449.

8. JET Team, in Proc. 15th Europ. Conf. on Controlled Fusion and Plasma Heating, Vol. 1, (Dubrovnik, Yugoslavia, 1987) p. 377.

9. PDX Group, Proc. in *Heating in Toroidal Plasmas,* Rome, 1984 (Int. School of Plasma Phys., Varenna, 1984) Vol. 2, p. 809.

10. R.M. Sillen, H.W. Pickaar, T. Oyevaar, E.P. Gozbunov, A.A. Bagdasorov, and N.L. Vasom, Nucl. Fusion **26**, 303 (1986).

11. DIII-D Group, 12th Int. Conf. on Plasma Phys. and Controlled Nuclear Fusion Research (Nice, France) IAEA-CN-50/E-I-2 (1988).

12. L. Chen, R.B. White, and M.N. Rosenbluth, Phys. Rev. Lett. **52**, 1122 (1984).

13. B. Coppi and F. Porcelli, Phys. Rev. Lett. **57**, 2272 (1986).

14. R.B. White, M.N. Bussac, and F. Romanelli, Phys. Rev. Lett. **62**, 539 (1989).

15. B. Coppi, R.J. Hastie, S. Migliuolo, F. Pegoraro, and F. Porcelli, Phys. Lett. **A132**, 267 (1988).

16. Y.Z. Zhang, H.L. Berk, and S.M. Mahajan, Nucl. Fusion, **29**, 847 (1989).

17. Y.Z. Zhang and H.L. Berk, Phys. Lett. **A 143**, 250 (1990).

18. R.B. White, F. Romanelli, and M.N. Bussac, Phys. Fluids **132**, 745 (1990).

19. Y.Z. Zhang, Bull. Am. Phys. Soc. **23**, 2074 (1988).

20. F. Pegoraro and T.J. Schep, Plasma Phys. and Controlled Fusion **28**, 647 (1986).

21. T.S. Hahm and L. Chen, Phys. Fluids **28**, 3061 (1985).

22. T.S. Hahm, Ph.D. Thesis, Princeton University, 1984.

23. F. Porcelli, Ph.D. Thesis, Suola Normale Superione, Pisa, Italy, 1987.

24. T.J. Schep, F. Pegoraro, and F. Porcelli, Proc. 15th Europ. Conf. on Controlled Fusion and Plasma heating, Dubrovnik (1988).

25. F. Pegoraro, F. Porcelli, and T.J. Schep, Phys. Fluids **B1**, 364 (1989).

26. T.M. Antonsen, Jr. and B. Coppi, Phys. Lett. **81A**, 335 (1981).

27. G.B. Crew, T.M. Antonsen, Jr., and B. Coppi, Nucl. Fusion **22**, 41 (1982).

28. S.C. Cowley, R.M. Kulsrud, and T.S. Hahm, Phys. Fluids **29**, 3230 (1986).

29. S.M. Mahajan, R.D. Hazeltine, H.R. Strauss, and D.W. Ross, Phys. Fluids **22**, 2147 (1979).

30. L. Chen, Private Communication.

Table I
Comparison of Numerical Δ_n with Δ_1, Δ_2, and Δ_4' for Various $\tilde{\sigma}$ and y_e^*

Δ_n	Δ_4'	Δ_1	Δ_2	$\tilde{\sigma}$	y_e^*
5.872	5.366	5.924	5.754	0.25	0.05
7.534	8.151	7.943	7.089	0.25	0.1
-42.617	-14.639	-11.528	506.489	0.25	0.25
-2.651	-2.586	-1.125	-3.155	0.25	0.5
-1.226	-1.418	-0.242	-1.404	0.25	0.75
-0.756	-0.977	0.066	-0.857	0.25	1.0
-0.257	-0.435	0.405	-0.291	0.25	2.0
-0.065	-0.163	0.539	-0.076	0.25	5.0
4.438	3.108	4.506	4.387	0.5	0.05
4.737	3.449	5.126	4.589	0.5	0.1
7.034	5.144	-10.126	6.173	0.5	0.25
-31.449	28.374	0.979	-855.61	0.5	0.5
-3.847	-8.070	1.456	-4.186	0.5	0.75
-1.881	-3.532	1.605	-1.840	0.5	1.0
-0.519	-1.087	1.750	-0.426	0.5	2.0
-0.117	-0.353	1.796	-0.080	0.5	5.0
3.817	2.065	3.767	3.795	1.0	0.05
3.895	2.135	3.690	3.827	1.0	0.1
4.407	2.378	2.897	4.122	1.0	0.25
7.026	2.933	-14.213	6.135	1.0	0.5
40.810	3.827	12.404	72.279	1.0	0.75
-8.308	5.503	9.628	-4.716	1.0	1.0
-1.098	-7.319	8.346	-0.505	1.0	2.0
0.213	-0.916	8.123	-0.058	1.0	5.0
3.501	1.430	3.489	3.489	2.0	0.05
3.523	1.446	3.486	3.493	2.0	0.1
3.693	1.498	3.445	3.551	2.0	0.25
4.350	1.593	3.140	4.052	2.0	0.5
5.896	1.701	2.311	6.566	2.0	0.75
10.750	1.824	0.696	-31.515	2.0	1.0
-2.923	2.572	-18.850	-0.442	2.0	2.0
-0.399	11.278	-345.57	-0.025	2.0	5.0

Figure Captions

1. Comparison of the numerically evaluated Δ^{-1}, with the rigorous asymptotic form Δ_1^{-1} and a fitted form Δ_2^{-1}. Figures (a) to (d) are for $\sigma = .25, .5, 1.0$, and 2.0, respectively. The solid curve corresponds to the numerical evaluation Δ_n^{-1}, the dashed curve to Δ_2^{-1} and the dotted curve to Δ_1^{-1}.

2. Marginal stability curves for Eq. (51) for various values of τ ($\tau = .1, .25, .5, 1.0, 2.0, 5.0$). In Figs. (a) and (b) the stability boundary curves for the normalized MHD energy vs. the parameter k_0 are presented. The arrows indicate that the marginal curves continue on $\delta\widetilde{W} = 0$ to $k_0 = 0$. Figure (c) shows the marginal frequency as a function of k_0.

3. Schematic diagrams of the stablity regions found for Eq. (51). The hatched regions are regions of stability.

4. The mode frequencies [Fig. 4(a)] and growth rates Fig. 4(b) of the dispersion relation, Eq. (51) for $\widetilde{\nu}_{ei} = 0.01, 0.1, 0.25$ (curves a, b, c) at $\delta\widehat{W}_c = -1 \times 10^{-3}$, $\widehat{\rho}_i = 0.01$, $\beta_i = 0.01$, and $\tau = 1.0$. The solid and dashed curves in Figs. a and b should be associated with each other.

5. The mode frequencies [Fig. 5(a)] and growth rates [Fig. 5(b)] of the MHD-like mode in the dispersion relation of Eq. (50) [or Eq. (A14)] for the kinetic electron conductivity given by Eq. (5) and Eq. (6) for $\eta_e = 0$, 1.0, 3.0 (curves a, b, c) at $\delta\widehat{W}_c = -1 \times 10^{-3}$, $\widehat{\rho}_i = 0.1$, $\beta_i = 0.01$, and $\tau = 1.0$. The solid and dashed curves in Figs. (a) and (b) should be associated with each other.

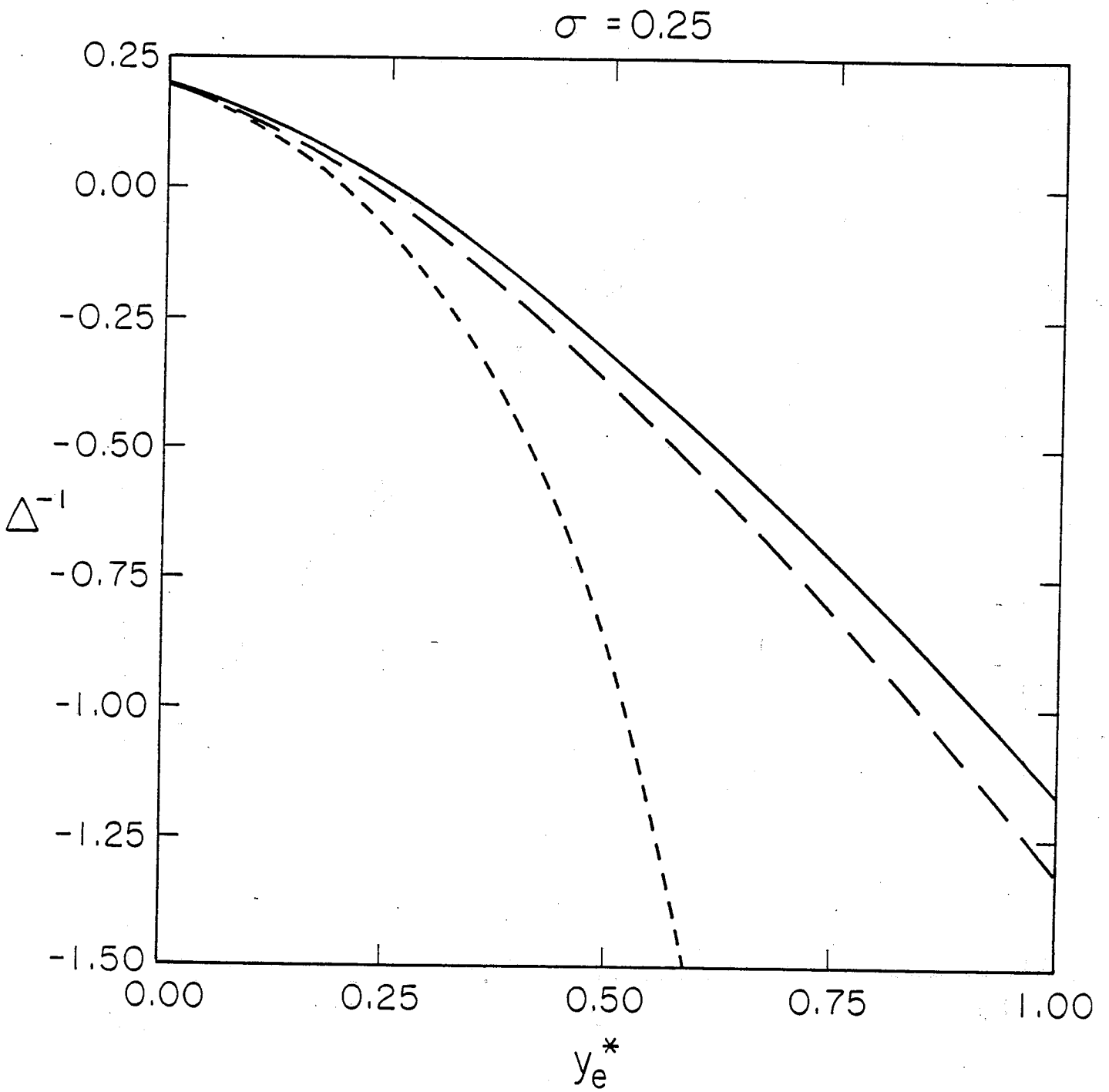

Fig. 1(a)

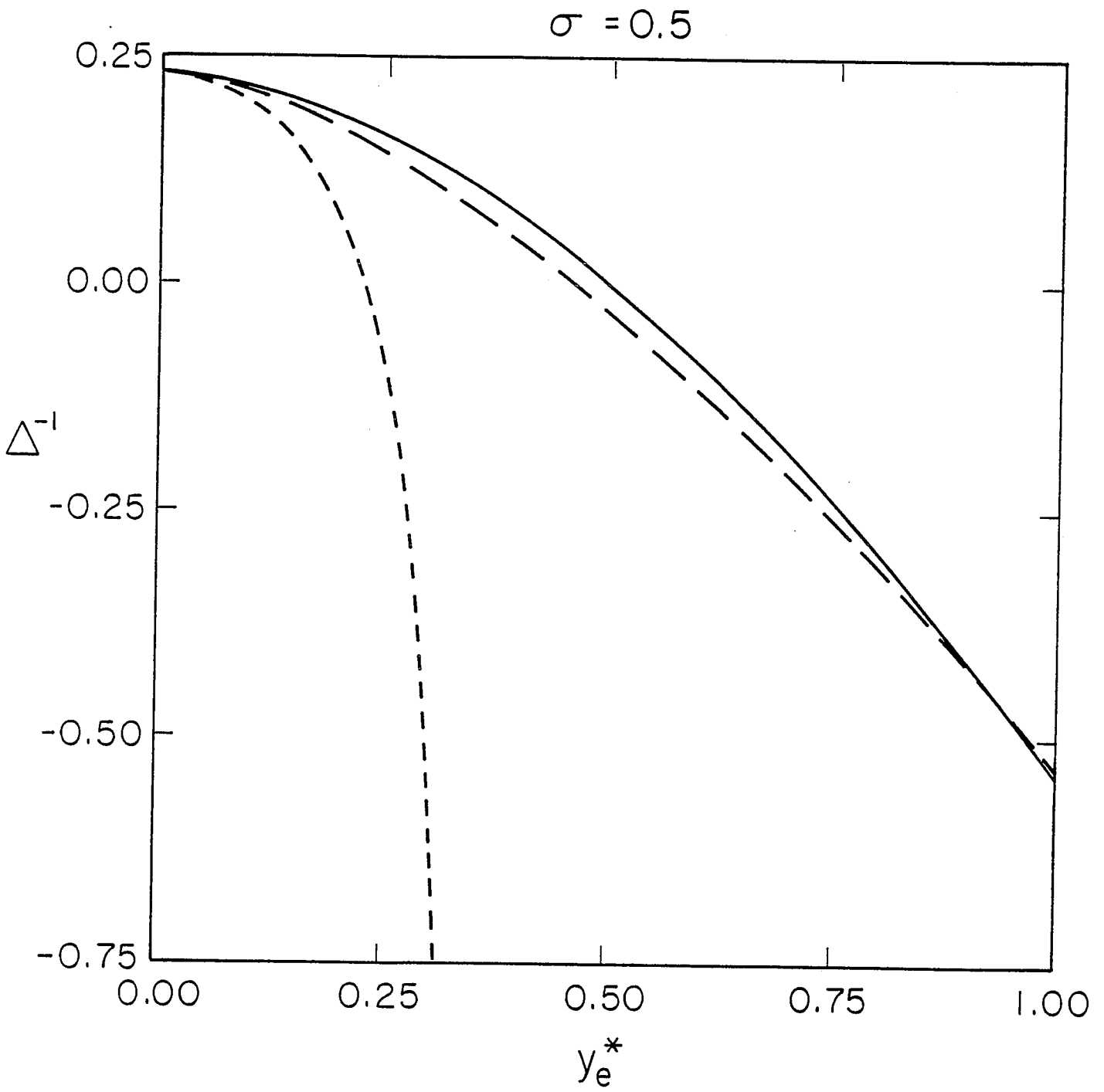

Fig. 1(b)

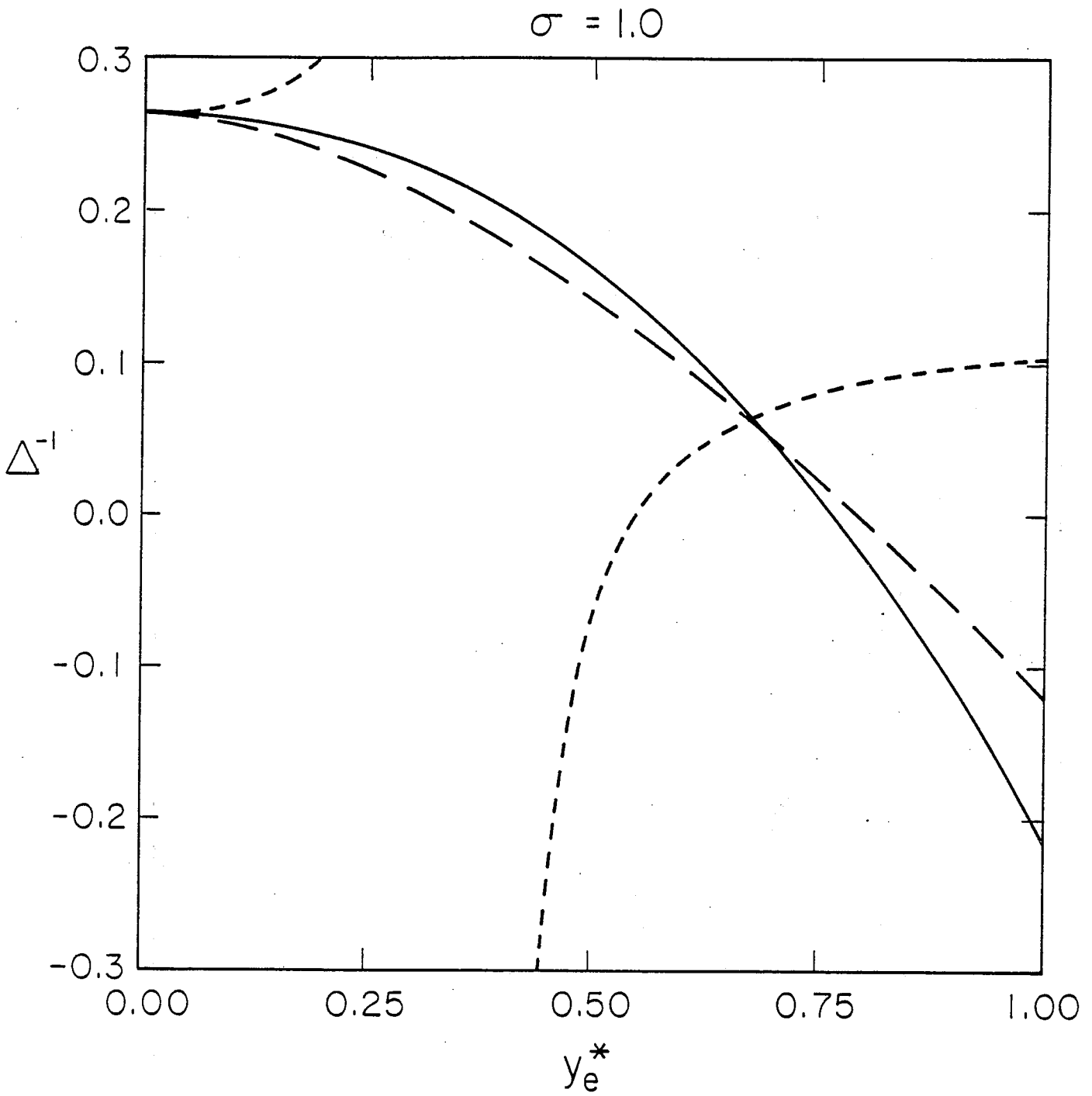

Fig. 1(c)

Fig. 1(d)

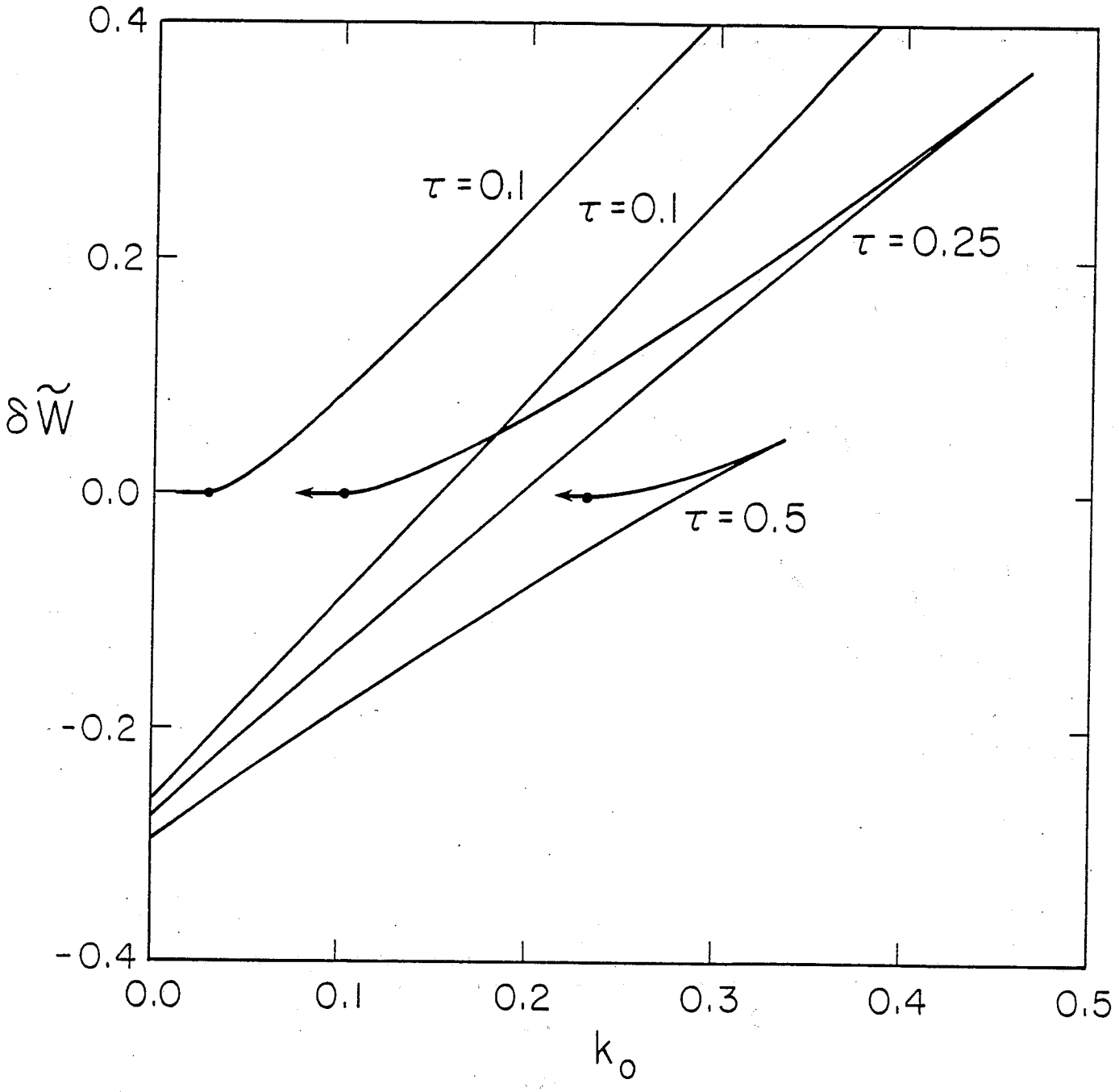
0.4
0.2
0.0
-0.2
-0.4
$\delta\tilde{W}$
$\tau = 0.1$
$\tau = 0.1$
$\tau = 0.25$
$\tau = 0.5$
0.0
0.1
0.2
0.3
0.4
0.5
k_o

Fig. 2(a)

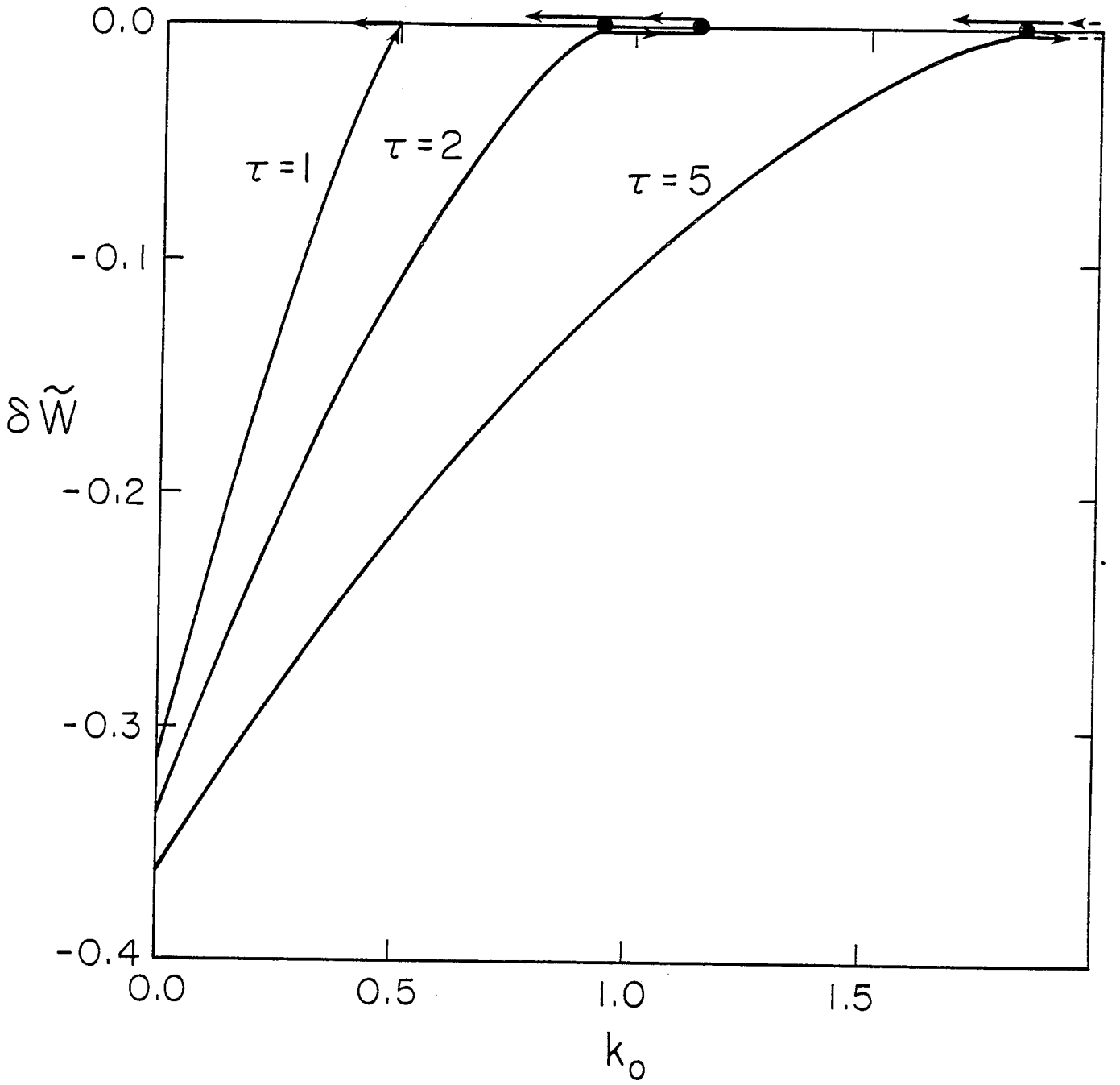

Fig. 2(b)

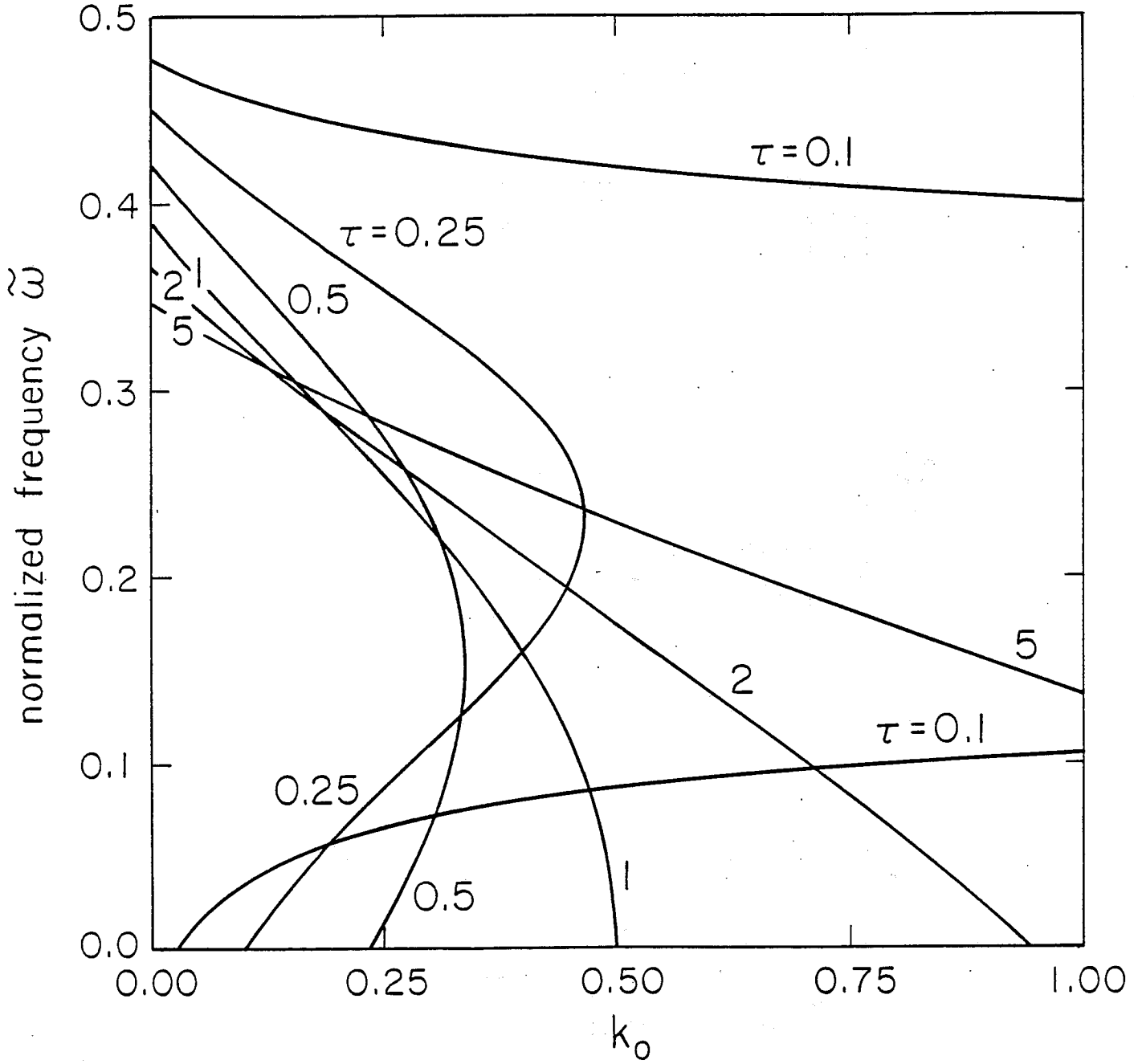
0.5
0.4
0.3
0.2
0.1
0.0
0.00
0.25
0.50
0.75
1.00
normalized frequency $\tilde{\omega}$
k_0
$\tau = 0.1$
$\tau = 0.25$
0.5
2
1
5
5
2
$\tau = 0.1$
0.25
0.5
1

Fig. 2(c)

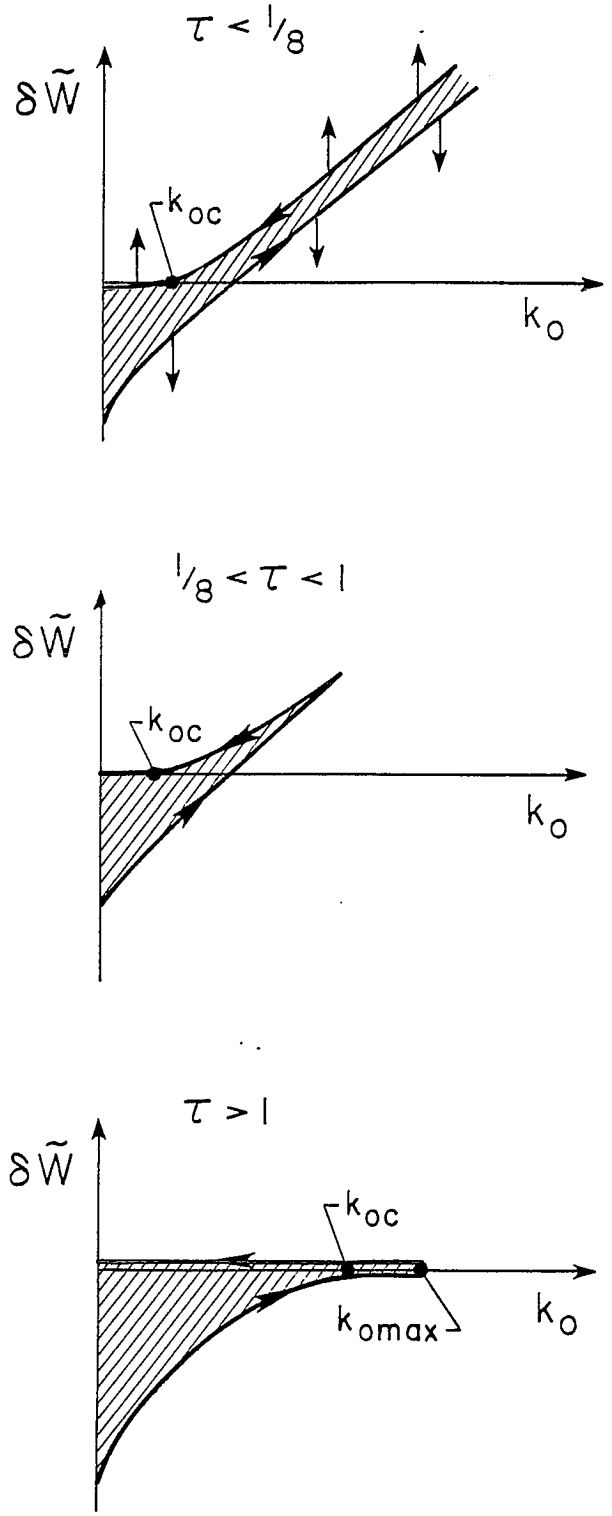

Fig. 3

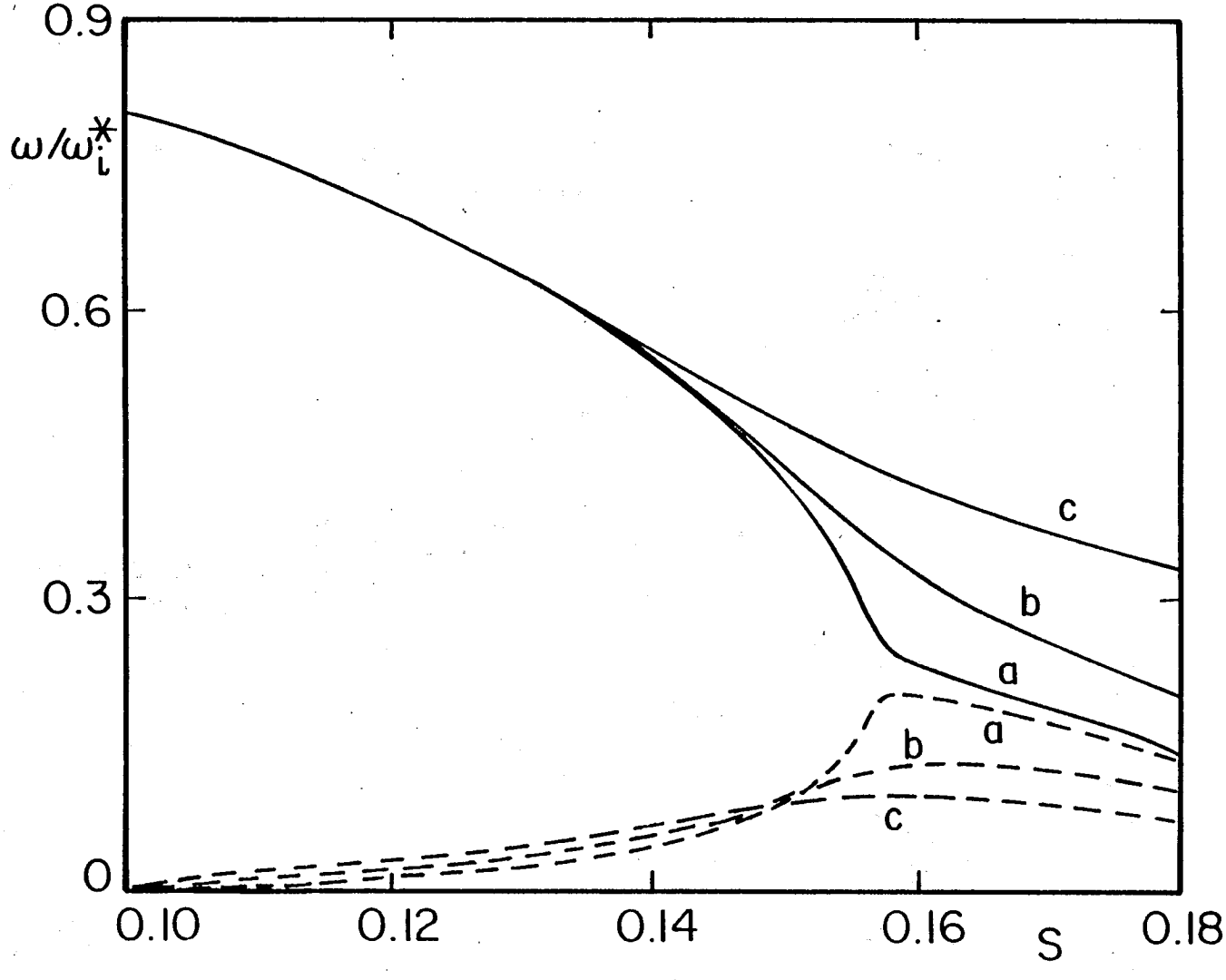

Fig. 4(a)

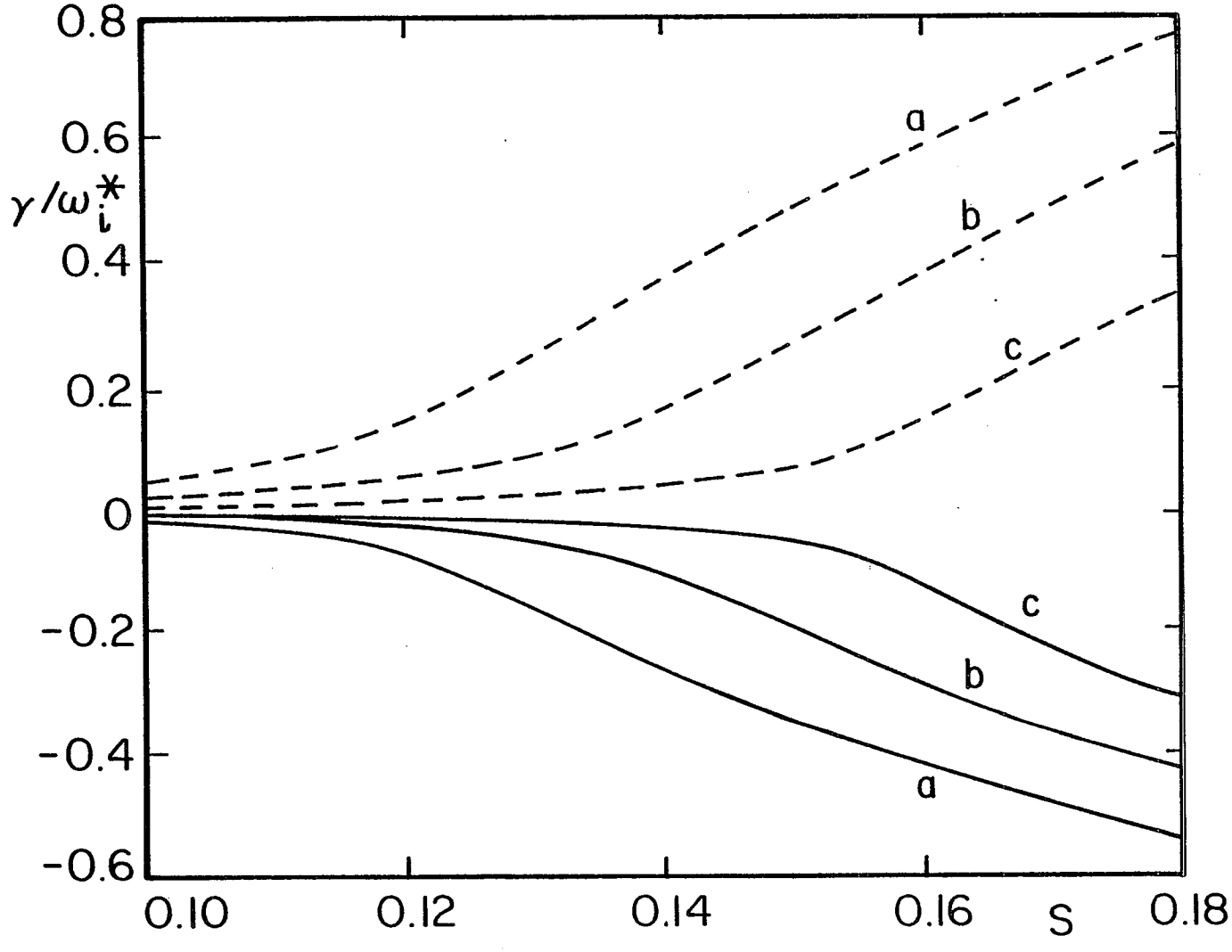

Fig. 4(b)

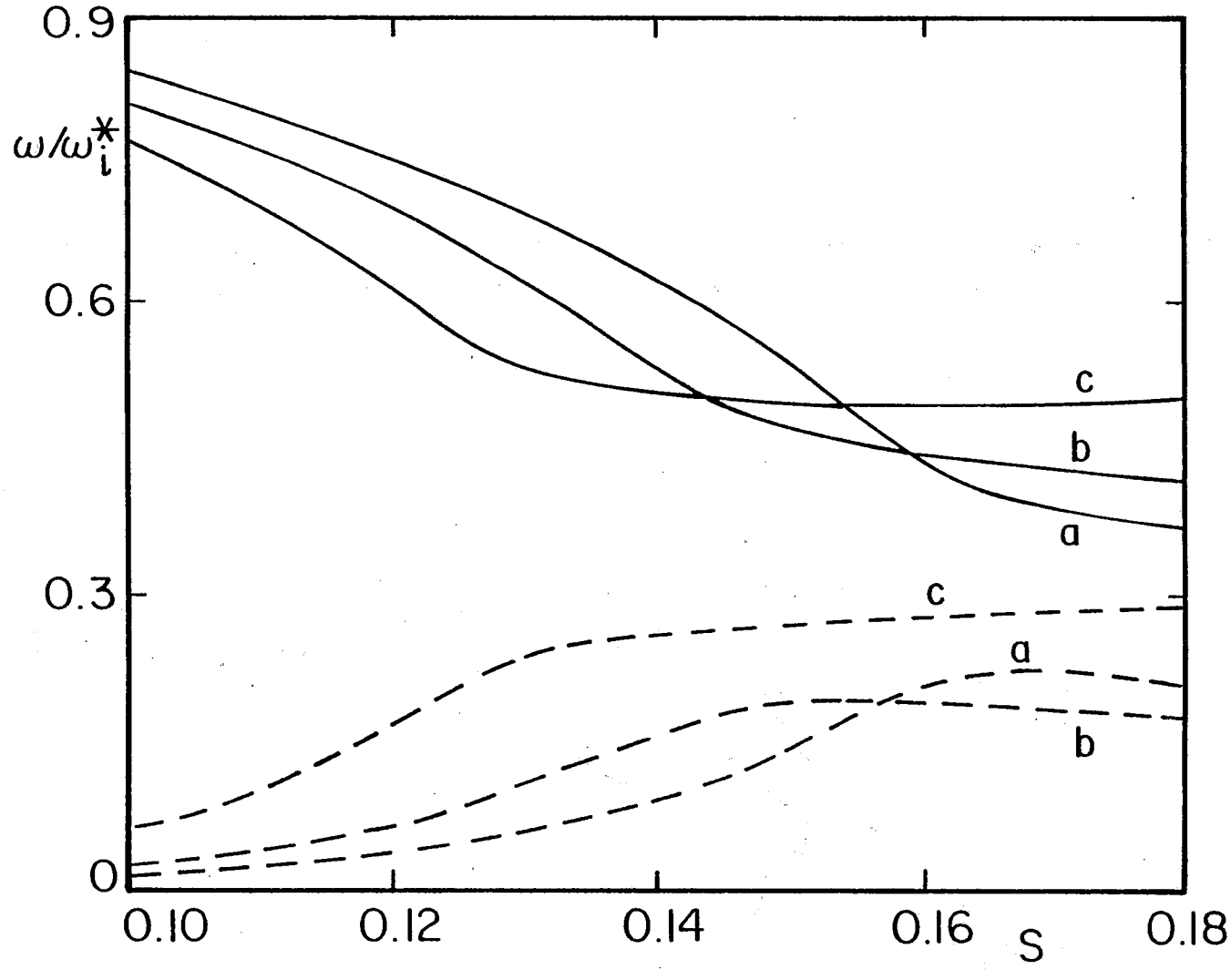

Fig. 5(a)

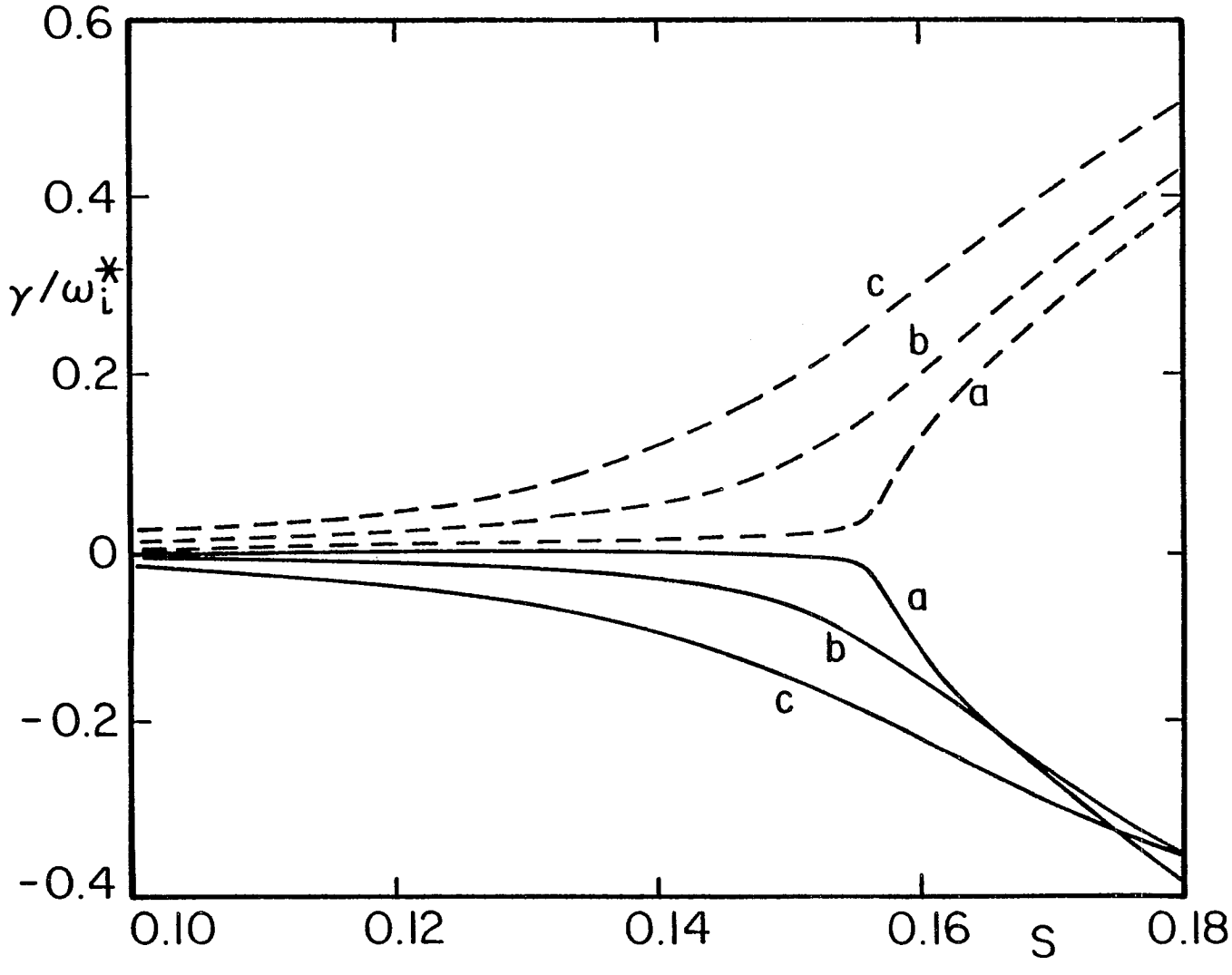

Fig. 5(b)